Journal of Cosmology and Astroparticle Physics
An IOP and SISSA journal

Gravitational wave production from preheating with trilinear interactions

Catarina Cosme, Daniel G. Figueroa and Nicolás Loayza

Instituto de Física Corpuscular (IFIC), Universitat de València-CSIC,
Parc Científic UV, C/ Catedrático José Beltrán 2, E-46980 Paterna, Spain

E-mail: catarina.cosme@ific.uv.es, daniel.figueroa@ific.uv.es,
nicolas.loayza@ific.uv.es

Received September 14, 2022
Revised March 3, 2023
Accepted April 4, 2023
Published May 10, 2023

Abstract. We investigate the production of gravitational waves (GWs) during preheating with monomial/polynomial inflationary potentials, considering a trilinear coupling $\phi\chi^2$ between a singlet inflaton ϕ and a daughter scalar field χ. For sufficiently large couplings, the trilinear interaction leads to an exponential production of χ particles and, as a result, a large stochastic GW background (SGWB) is generated throughout the process. We study the linear and non-linear dynamics of preheating with lattice simulations, following the production of GWs through all relevant stages. We find that large couplings lead to SGWBs with amplitudes today that can reach up to $h^2\Omega^{(0)}_{\rm GW} \simeq 5\cdot 10^{-9}$. These backgrounds are however peaked at high frequencies $f_{\rm p} \gtrsim 5\cdot 10^6$ Hz, which makes them undetectable by current/planned GW observatories. As the amount of GWs produced is in any case remarkable, we discuss the prospects for probing the SGWB indirectly by using constraints on the effective number of relativistic species in the universe $N_{\rm eff}$.

Keywords: physics of the early universe, primordial gravitational waves (theory), gravitational waves / sources, particle physics - cosmology connection

ArXiv ePrint: 2206.14721

https://doi.org/10.1088/1475-7516/2023/05/023

JCAP05(2023)023

Contents

1 Introduction

Significant evidence [1] supports the idea of inflation as a solution to the shortcomings of the hot Big Bang framework [2–4], and as a mechanism to create the primordial density perturbations [5–9] (see [10–14] for reviews on inflation). Inflationary models must be compatible with cosmological observations [1, 15], including the most recent constraint on the B-mode polarization of the Cosmic Microwave Background (CMB), which sets an upper bound on the inflationary Hubble scale as $H_{\rm inf} \lesssim 4.7 \times 10^{13}\,\text{GeV}$ [16]. This rules out many scenarios, and puts pressure on the parameter space of many others.

Inflation must be followed by a period of *reheating* during which the Universe ultimately has to reach a radiation dominated (RD) thermal state, at least before the onset of Big Bang Nucleosynthesis (BBN) at a temperature of $T_{\rm BBN} \simeq 10^{-3}$ GeV [17–20]. The first stage of reheating may be driven by a period of *preheating*, characterized by strong non-perturbative field excitation, typically leading to exponentially growing particle number densities. A paradigmatic example of this is parametric resonance, a phenomenon by which particle species coupled to the inflaton — the *daughter* fields –, are created in energetic bursts due to the oscillations of the inflaton around the mininum of its potential. In the case of bosonic species, the production of daughter particles is resonant, and the energy transferred into them grows exponentially within few inflaton oscillations [21–28]. Other preheating mechanisms include particle creation due to trilinear or higher-order interactions between the inflaton and daughter field(s) [29–32], geometric preheating of fields non-minimally coupled to gravity [33–36], tachyonic preheating after Hybrid inflation of Higgs-like fields [37–40] and of gauge fields [41–51], gauge field excitation due to shift-symmetric interactions with an axion-like inflaton [52–55], etc. Multi-field (p)reheating scenarios have been also considered [56–60], including the case with non-minimal gravitational couplings [61–65]. For reviews on (p)reheating we refer the reader to [66–69].

A common byproduct of early universe dynamics are gravitational waves (GWs). A (quasi-)scale invariant stochastic GW background (SGWB) is actually predicted in vanilla

JCAP05(2023)023

models due to quantum vacuum fluctuations [70–75], whereas the dynamics of axion-like species during inflation generate blue-tilted signals [76–89]. SGWBs are also expected from post-inflationary phenomena, like particle production during preheating [50, 54, 90–99], oscillon dynamics [100–104], kination-dynamics [105–111], and others. For reviews on SGWBs of cosmological origin see [112, 113]. In this work, we focus on GW production during preheating.

While many preheating studies have considered four-leg interactions $\phi^2\chi^2$ of the inflaton ϕ with another scalar field χ, the inflaton can never decay completely in such a case [25, 114–117]. To allow for a complete inflaton decay, interactions of the form $\phi\chi^n$ must be included. Trilinear interactions with $n = 2$ are simply the most natural choice, as interactions of this type are ubiquitous in particle physics. A paradigmatic example are Yukawa interactions, which represent a coupling between a scalar and two fermions. Three-leg decay via fermions was in fact the first channel of inflaton perturbative decay considered [118, 119], though it was realized later on that the inflaton also decays via non-perturbative parametric excitations in that case [120–123]. Three-leg decay via interactions with bosons leads also to non-perturbative parametric excitations [29], and this channel is actually expected to dominate over Yukawa interactions, simply due to Pauli blocking of the Fermions. Furthermore, theories with spontaneous symmetry breaking or scalar theories charged under gauge symmetries, lead naturally to trilinear vertices between bosonic species, often involving gauge fields. Even if we restrict ourselves to scalar field interactions, trilinear interactions are naturally expected in many contexts. A trilinear interaction $\phi\chi^2$ between an inflaton ϕ and a scalar daughter field χ represents therefore a natural coupling between an inflationary sector and a matter sector, and hence we focus on this type of interaction in this paper.

Considering in particular the interaction term $\frac{1}{2}\sigma\phi\chi^2$, where σ is a coupling of mass dimensions, we can understand the excitation mechanism underlying this interaction as follows. If following the end of inflation the inflaton oscillates coherently around the origin of its potential, the effective oscillatory frequency of a χ-field mode function χ_k is given by $\omega_k^2(t) = \frac{k^2}{a^2} + m_\chi^2 + \sigma\,\phi\,(t)$, with k the modulus of the comoving momentum, and $a(t)$ the scale factor. If the bare mass of χ satisfies $m_\chi^2 \ll \sigma\,|\phi|$, the trilinear coupling will induce a tachyonic mass for χ whenever $\phi < 0$, which happens during half of the time of each inflaton oscillation. Correspondingly, the modes within the infrared (IR) window $k^2 < \sigma\,|\phi|\,a^2$ will be exponentially amplified periodically, every half-period of the inflaton oscillations. This resonant mechanism, dubbed *tachyonic resonance* in ref. [29], leads to a very efficient production of χ particles, so preheating concludes within few oscillations of ϕ.

If the daughter field χ is the Standard Model (SM) Higgs, the question of the stability of its vacuum becomes of upmost relevance. Even though the presence of a trilinear coupling does not affect the stability of the Higgs vacuum during inflation, it can influence it during preheating [124]. If the trilinear coupling σ is large enough, the exponentially large occupation number of the Higgs created by tachyonic resonance can destabilize the vacuum. Lattice simulations have set upper bounds on the value of the trilinear coupling σ, and on the dimensionless coupling of a scale-free interaction $\frac{1}{2}\lambda_{h\phi}\phi^2h^2$, based on demanding a stable evolution of the Higgs during preheating. According to ref. [32], Higgs vacuum stability is assured whenever the couplings respect the bounds $10^{-10} < \lambda_{h\phi} < 10^{-8}$ and $\sigma < 2\times10^8$ GeV.

In our present work we consider a daughter field χ with its self-interaction coupling strictly positive.[1] The excitation of the field modes χ_k within the aforementioned IR tachyonic

[1] In other words, χ could be identified with the SM Higgs only if the self-interaction coupling λ of the Higgs remains positive at large scales, something that depends (in the absence of beyond the SM physics) very sensitively on the choice of α_s and the top Yukawa coupling y_t [125, 126].

JCAP05(2023)023

window provides a non-trivial time-dependent spatial configuration for $\chi(\mathbf{x}, t)$, which in turn generates gravitational radiation. Here we study for the first time the GW production during preheating with a trilinear interaction $\frac{1}{2}\sigma\phi\chi^2$. We consider different inflaton potentials $V_{\rm inf}(\phi)$ with minimum at the origin, and study the GW production during preheating in each case, as a function of σ. As the periodic tachyonic excitation of the IR modes χ_k resembles to some extent the excitation of gauge fields during preheating after axion-inflation [52, 53], and the latter is known to source GWs very efficiently [54, 55, 99], we expect a very efficient GW production due to the trilinear coupling. We investigate therefore whether we may obtain SGWBs such that their energy density could be constrained by upper bounds on the number of relativistic species in the universe [127–131], hence placing constraints on σ. Furthermore there is also the possibility that due to the nature of the trilinear interaction, the frequencies of the expected SGWB could be shifted towards smaller (more observable) frequencies than the SGWBs produced in standard $\phi^2\chi^2$ preheating [97].

The paper is divided as follows. In section 2, we analyse the preheating dynamics and GW production for a monomial inflaton potential. In section 3, we study the preheating dynamics and GW production for a polynomial inflaton potential. In section 4, we summarise our results and their potential implications. Some technical details are given in the appendices.

Conventions. We consider a spatially-flat Friedmann-Lemaitre-Robertson-Walker (FLRW) background metric, $ds^2 = -dt^2 + a(t)^2\delta_{ij}dx^i dx^j$, where $a(t)$ is the scale factor, and t the cosmic time. We assume summation over repeated indices. On top of the background we consider tensor metric perturbations that satisfy $h_{ii} = \partial_i h_{ij} = 0$, hence identified with GWs. We denote the reduced Planck mass by $m_p = 2.435 \cdot 10^{18}$ GeV.

2 Monomial potential

We start our investigation by considering a quadratic potential for the inflaton ϕ around the origin. While a purely monomial potential $V_{\rm inf}(\phi) \propto \phi^2$ for inflation is strongly disfavored[2] by CMB B-mode data [16], we can consider consistent inflaton potentials that flatten out towards large field values by developing a plateau, and then adopt a monomial shape around the origin only after inflation ends. These potentials are inspired by α-attractor models [133] and can be written as $V_{\rm inf}(\phi) = \frac{1}{2}\Lambda^4 \tanh^2(\phi/M)$, where M and Λ constants have dimensions of mass. In the limit $|\phi| \ll M$, the potential becomes $V_{\rm inf}(\phi) \simeq \frac{1}{2}m_\phi^2\phi^2$, with $m_\phi^2 \equiv \Lambda^2/M$. Compatibility with CMB observations at CMB scales allow us to choose $M = 5m_p$, which then leads to $\Lambda = 0.00564 m_p$, and from there to an inflaton mass $m_\phi \simeq 1.6 \cdot 10^{13}$ GeV (see e.g. section II of ref. [116] for further details). Finding m_ϕ from fitting CMB anisotropy observables with an inflationary quadratic potential $V_{\rm inf}(\phi) = \frac{1}{2}m_\phi^2\phi^2$ at CMB scales, leads however to a very similar scale for the inflaton mass as in the α-attractor case. So, in practice, we then simply consider a quadratic potential for the inflaton ϕ, and supplement it with a trilinear interaction $\phi\chi^2$ with a daughter scalar field χ, for which we allow self-interactions,

$$V(\phi, \chi) = \frac{1}{2}\, m_\phi^2\, \phi^2 + \frac{\sigma}{2}\, \phi\, \chi^2 + \frac{\lambda}{4}\chi^4, \tag{2.1}$$

where σ is a coupling with dimensions of mass, and λ is the self-interaction coupling of the daughter field. We neglect a term $\frac{1}{2}\, m_\chi^2\, \chi^2$ in eq. (2.1) as we anticipate that the typical

[2] Monomial potentials during inflation are not ruled out if an appropriate non-minimal coupling between the inflaton and the Ricci scalar is also present [132].

JCAP05(2023)023

momenta excited $k/a \lesssim \sigma|\phi|$ will be very large, and hence we simply assume that $m_\chi \ll \sigma|\phi|$. It is however necessary to include the χ^4 self-interaction to ensure that the potential is bounded from below and, consequently, only stable dynamics are developed. We then identify a *critical* coupling

$$\lambda_c(\sigma, m_\phi) \equiv \frac{\sigma^2}{2\, m_\phi^2}\,, \tag{2.2}$$

so that values $\lambda < \lambda_c$ are not allowed because the potential in eq. (2.1) would not be bounded from below. The critical value λ_c defines in fact a flat direction $\phi = -\frac{\sigma\,\chi^2}{2\,m_\phi^2}$, where $V(\phi, \chi) = 0$. For $\lambda > \lambda_c$ the flat direction is lifted and the potential has a minimum at $\phi = \chi = 0$ where $V(\phi, \chi) = 0$. The requirement that the potential has to be bounded from below thus imposes an important relation between the two couplings of the model, σ and λ. Throughout our following analysis, we adopt a value $\lambda = 2\lambda_c$ so that our numerical dynamics are guaranteed to avoid running-away solutions.

2.1 Preheating dynamics. Lattice simulations

The dynamics of preheating depend on the curvature of the potential around its minimum, so our results hold for a class of inflationary models with similar effective inflaton potential around the origin, as long as the leading term is quadratic. As mentioned before, the monomial inflaton potential that we considered in eq. (2.1), $V_{\rm inf}(\phi) = \frac{1}{2}\, m_\phi^2\, \phi^2$, is simply a very good approximation to the α-attractor potential $V_{\rm inf}(\phi) = \frac{1}{2}\Lambda^4 \tanh^2(\phi/M)$ at field amplitudes $|\phi| \ll M$. For simplicity in our analysis, we will fix the initial amplitude $\Phi_{\rm i}$ of the inflaton at the beginning of preheating (onset of inflaton oscillations), by determining the end of inflation in a quadratic inflaton potential $V_{\rm inf}(\phi) \propto \phi^2$. Following the end of inflation, the inflaton (in the form of a homogeneous condensate) starts oscillating around the origin. During the oscillatory stage, the inflaton produces copiously particles of the χ field, transferring exponentially energy into the new quanta created. In our model, preheating occurs via a trilinear interaction, which provides an effective time-dependent mass term for χ with oscillatory sign in time. Whenever $\phi < 0$, which occurs during half the time of each inflaton oscillation, the trilinear coupling provides a negative squared mass for χ. Hence, the corresponding χ_k modes will be exponentially enhanced periodically, every time that $\phi < 0$. This mechanism, known as tachyonic resonance, leads to a very efficient production of χ particles after few oscillations of ϕ [29, 32].

The system is fully characterized by the following set of equations,

$$\ddot{\phi} + 3\,H\,\dot{\phi} + m_\phi^2\phi + \frac{\sigma}{2}\,\chi^2 - \frac{\nabla^2\phi}{a^2} = 0\,, \tag{2.3}$$

$$\ddot{\chi} + 3\,H\,\dot{\chi} + \lambda\,\chi^3 + \sigma\,\chi\,\phi - \frac{\nabla^2\chi}{a^2} = 0\,, \tag{2.4}$$

where $a(t)$ is the scale factor and $H \equiv \dot{a}/a$ the Hubble rate. Before we move into a lattice formulation of eqs. (2.3)–(2.4), in order to get some preliminary insight about tachyonic resonance, we will first consider the linear regime, where the inflaton ϕ will be treated as a homogeneous background field. In order to do this, we start by a change of variables

$$d\tilde{x}^\mu = m_\phi\, dx^\mu\,, \quad \tilde{\phi} = \frac{\phi}{\Phi_i}\,, \quad \tilde{\chi} = \frac{\chi}{\Phi_i}\,, \quad \tilde{H} = \frac{H}{m_\phi}\,, \tag{2.5}$$

JCAP05(2023)023

and then move into Fourier space, where we can naturally quantize the field χ as usual, writing

$$\tilde{\chi}(\mathbf{x},t) = \int \frac{d^3\mathbf{k}}{(2\pi)^3}[\hat{a}_k \tilde{\chi}_k(t) e^{i\mathbf{k}\cdot\mathbf{x}} + \hat{a}^\dagger \tilde{\chi}_k^*(t) e^{-i\mathbf{k}\cdot\mathbf{x}}]\,, \tag{2.6}$$

with $\hat{a}_k^\dagger$, $\hat{a}_k$ standard creation/annihilation operators that satisfy $[\hat{a}_k, \hat{a}_{k'}^\dagger] = (2\pi)^3\delta(\mathbf{k}-\mathbf{k}')$. The evolution equation of the mode functions $\tilde{\chi}_k$, can be written as a linear equation using the Hartree approximation $\tilde{\chi}^3 \to 3\,\tilde{\chi}\,\langle\tilde{\chi}^2\rangle$ in eq. (2.4), so that

$$\tilde{\chi}_k'' + 3\,\tilde{H}\tilde{\chi}_k' + \left(3\,q_\chi\left\langle\tilde{\chi}^2\right\rangle + q_3\,\tilde{\phi}\,(t) + \frac{\kappa^2}{a^2}\right)\tilde{\chi}_k = 0\,, \qquad \text{with} \quad \kappa = \frac{k}{m_\phi}\,, \tag{2.7}$$

where prime $'$ denotes derivatives with respect to the new time variable, and the variance $\langle\tilde{\chi}^2\rangle$ can be related to the *power spectrum* of χ as follows

$$\langle\tilde{\chi}^2\rangle = \int d\log k\,\Delta_\chi(k)\,, \quad \Delta_\chi(k) \equiv \frac{k^3}{2\pi^2}\mathcal{P}_\chi\,, \quad \langle\chi_{\mathbf{k}}\chi^*_{\mathbf{k}'}\rangle \equiv (2\pi)^3\mathcal{P}_\chi(k)\delta(\mathbf{k}-\mathbf{k}')\,. \tag{2.8}$$

We note that in eq. (2.7) two dimensionless *resonance parameters* have naturally emerged,

$$q_3 \equiv \frac{\sigma\,\Phi_i}{m_\phi^2} \quad \text{and} \quad q_\chi \equiv \frac{\lambda\,\Phi_i^2}{m_\phi^2}\,, \tag{2.9}$$

with Φ_i the initial amplitude of the homogeneous field at the end of inflation. These parameters, as we will see later, play a fundamental role in our model, as they control the intensity of the daughter field excitation. Looking at the mode frequency in eq. (2.7), we can write

$$\tilde{\omega}_k^2 = m_{\tilde{\chi}}^2 + (\kappa/a)^2\,, \qquad m_{\tilde{\chi}}^2 = \left(q_3\,\tilde{\phi}\,(t) + 3q_\chi\langle\tilde{\chi}^2\rangle\right). \tag{2.10}$$

As the inflaton field oscillates in a quadratic potential as $\tilde{\phi}\,(t) \simeq \Phi(t)\sin(m_\phi\,t)$, with $\Phi(t) \propto \frac{1}{t} \propto \frac{1}{a^{3/2}}$ [134], we see that literally during every half oscillation the inflaton amplitude becomes negative. Hence, from eq. (2.10), we can see that every time that $\phi < 0$, $\tilde{\omega}_k^2$ becomes negative for sufficiently infrared momenta with modulus below the cut-off $\kappa^2 < -m_{\tilde{\chi}}^2$. This leads to an exponential growth of such infrared modes $\tilde{\chi}_k$, which translates at the same time into an exponential growth of the variance $\langle\tilde{\chi}^2\rangle$ (or equivalently into an exponential growth of the power spectrum $\mathcal{P}_\chi(k)$ of the IR modes). Such exponential growth must actually happen in a step-like manner, as every time the inflaton amplitude is negative we expect the variance to grow, whereas every time the inflaton is positive we expect the variance to oscillate (simply due to the mode oscillations when $\tilde{\omega}_k^2 > 0$ for $\phi > 0$). An overall exponential growth in steps is then expected.

In order to study the non-linear dynamics of the subsequent stages of the field excitation, we switch to using lattice simulations. In this work, we have considered the set of equations eq. (2.3) and eq. (2.4) and solved numerically a discrete version of them using `CosmoLattice` [135, 136]. The initial conditions for the homogeneous part of the inflaton field during inflation is obtained by solving the Friedmann equation $H^2 \equiv \left(\frac{\dot{a}}{a}\right)^2 = \frac{1}{3m_p^2}\left(\frac{1}{2}\dot{\phi}^2 + V(\phi)\right)$, together with eq. (2.3) in the absence of the χ field (as well as in the absence of the $\nabla^2\phi$ term). We obtain the initial amplitude and velocity from the breaking of slow roll condition, $\epsilon_H \equiv -\frac{\dot{H}}{H^2} = 1$, which leads to the homogeneous initial condition

$$\Phi_i \equiv \phi(t_i) = 1.00738\,m_p \quad \text{and} \quad \dot{\Phi}_i \equiv \dot{\phi}\,(t_i) = -0.712295\;\; m_\phi\,m_p\,. \tag{2.11}$$

JCAP05(2023)023

In the non-linear regime, the inflaton field will become fully inhomogenous $\tilde{\phi}(\mathbf{x}, t)$, so whenever we want to extract its homogeneous part we will do so by means of a volume average $\langle\tilde{\phi}\rangle$. The initial conditions for the χ field are such that the homogeneous amplitude is set to zero, and standard quantum vacuum fluctuations are added on top, following the standard recipe for initial lattice power spectra, see e.g. section 7 of ref. [135] for details.

We have performed a series of simulations with $N = 512$ lattice sites per dimension and a minimum infrared momentum $\kappa_{\rm IR} \in [0.2 : 0.75]$, where $\kappa_{\rm IR} = \frac{2\pi}{L}$ with L the comoving length of the lattice, making sure we capture well all relevant scales of the problem. Simulations were run for different values of q_3 while considering the relation $q_\chi = q_3^2$ for $q_3 \in [1 : 10^4]$. Such relation between the resonance parameters simply implies that we are using $\lambda = 2\lambda_c$, in order to be sufficiently safe from run-away solutions in the numerical dynamics. Simulations were forced to end at time $m_\phi t_{\rm f} = 400$, as by this time in all cases (independently of the coupling σ), the system has reached a steady state with no further energy exchange between fields.

We now explain the dynamics we identify in our lattice simulations. An initial stage is characterized by the oscillations of the inflaton, which remains as a homogeneous field for as long as the backreaction of the χ field can be neglected. In this regime, the solution to the equation of motion of the inflaton is $\phi(t) \simeq \sqrt{\frac{8}{3}}\frac{m_p}{m_\phi t}\cdot\sin(m_\phi t)$ [25]. The effective frequency of oscillation of the modes χ_k, as given in eq. (2.7), is negative whenever the inflaton is negative, which induces an exponential growth of the modes below the cut-off

$$\kappa < \sqrt{q_3|\tilde{\phi}|}\, a\,. \tag{2.12}$$

Looking at the mode frequency squared $\tilde{\omega}_k^2$ in eq. (2.10), we naturally identify an effective tachyonic resonance parameter as $q_{3,\rm eff} = q_3|\tilde{\phi}|$, with q_3 the initial resonance parameter defined in eq. (2.9). Due to the expansion of the universe, the inflaton envelope amplitude $\Phi(t)$ decays in time, and hence the effective resonance parameter decreases in time following the same decay as $q_{3,\rm eff} \propto |\Phi| \propto \frac{1}{a^{3/2}}$. Once the value of $q_{\rm eff}$ drops below 1/3, the system switches to a narrow resonance regime [29], where the tachyonic excitation is no longer effective. Hence, depending on the value of the trilinear coupling, two regimes can be identified: *i*) For 'small' values of q_3, $q_{3,\rm eff}$ drops below 1/3 before or soon enough after the first zero-crossing of the inflaton, and hence the growth of the variance of χ shuts down at a maximum value $\langle\tilde{\chi}^2\rangle_{\rm max}$ determined by the moment when $q_{3,\rm eff} = 1/3$, as shown in the *Left* panel of figure 1. *ii*) For 'large' values of q_3, the variance $\langle\tilde{\chi}^2\rangle$ grows exponentially in steps (as many as negative semi-cycles of the inflaton) up to a new larger maximum value $\langle\tilde{\chi}^2\rangle_{\rm max}$, which is reached before $q_{3,\rm eff}$ drops below 1/3. We refer to this new maximum as the *critical* value of the variance, $\langle\tilde{\chi}^2\rangle_{\rm max} = \langle\tilde{\chi}^2\rangle_{\rm crit}$, see *Right* panel of figure 1. In this second case, just about when the variance reaches $\langle\tilde{\chi}^2\rangle_{\rm crit}$, the backreaction of the daughter field into the inflaton cannot be ignored any longer. In particular, the growth of $\langle\tilde{\chi}^2\rangle$ towards $\langle\tilde{\chi}^2\rangle_{\rm crit}$ displaces the position of the minimum of the inflaton potential, so the inflaton is 'locked' to be around a negative value after the variance of χ reaches $\langle\tilde{\chi}^2\rangle_{\rm crit}$.

Numerically, we find the division between the two regimes to be at around $q_3 \simeq 10$, i.e. the regime *i*) of 'small' q_3 values corresponds to $q_3 < 10$, whereas the regime *ii*) of 'large' q_3 values corresponds to $q_3 > 10$. Although the maximum value $\langle\tilde{\chi}^2\rangle_{\rm max}$ corresponds in both regimes to the end of the tachyonic resonance, in the regime *i*) such value is reached when the condition $q_{3,\rm eff} \leq 1/3$ is satisfied, whereas in the regime *ii*) the maximum value corresponds to the moment when the χ self-interaction overtakes the trilinear interaction for the first time in χ's effective mass $m_{\tilde{\chi}}^2 = q_3\langle\tilde{\phi}\rangle + 3q_\chi\langle\tilde{\chi}^2\rangle$. By cancelling out the two terms with each other

JCAP05(2023)023

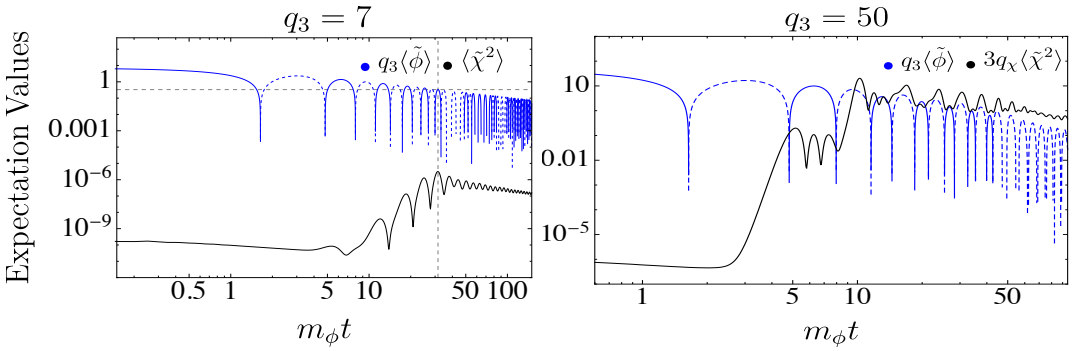

Figure 1. *Left*: Time evolution of the inflaton's volume average $\langle\tilde{\phi}\rangle$ times the resonance parameter q_3 ($q_{3\,\mathrm{eff}} = q_3\langle\tilde{\phi}\rangle$), and the variance of the daughter field $\langle\tilde{\chi}^2\rangle$ for $q_3 = 7$. The horizontal dashed line corresponds to $q_{3\,\mathrm{eff}} = 1/3$, whereas the vertical dashed line represents the time at which the maximum value of the variance is reached, $\langle\tilde{\chi}^2\rangle_{\mathrm{max}}$. *Right:* Time evolution of $q_3\langle\tilde{\phi}\rangle$ and the variance of the daughter field $\langle\tilde{\chi}^2\rangle$ times $3\,q_\chi$ for $q_3 = 50$. We see that once the term $3\,q_\chi\langle\tilde{\chi}^2\rangle$ overtakes $q_3\langle\tilde{\phi}\rangle$, the growth of the variance stops. For both panels, the solid (dashed) blue lines correspond to the positive (negative) part of the inflaton mean value.

(when $\tilde{\phi} < 0$), we can obtain an analytical estimation for the critical value $\langle\tilde{\chi}^2\rangle_{\mathrm{crit}}$ in the regime *ii*) as

$$\langle\tilde{\chi}^2\rangle_{\mathrm{crit}} \simeq \frac{q_3|\langle\tilde{\phi}\rangle|}{3q_\chi}\,, \qquad (q_3 \gtrsim 10)\,. \tag{2.13}$$

In figure 1, we show the time evolution of the mean value of the inflaton times the resonance parameter, $q_3\langle\tilde{\phi}\rangle$, and the variance of the daughter field $\langle\tilde{\chi}^2\rangle$, for $q_3 = 7$ (*Left* panel) and $q_3 = 50$ (*Right* panel), and for q_χ values that satisfy the relation $q_\chi = q_3^2$. Using the definitions of q_3 and q_χ in eqs. (2.9), we can easily see that the critical relation between σ and λ in eq. (2.2) translates into $q_\chi{=}\frac{q_3^2}{2}$. Thus, the relation $q_\chi = q_3^2$ used represents simply a conservative choice to avoid a possible runaway unstable solution of the dynamics, as mentioned before. As expected, we observe that $\langle\tilde{\chi}^2\rangle$ grows every negative semi-oscillation, whereas it oscillates during the positive ones. The variance stops growing once it reaches its maximum value $\langle\tilde{\chi}^2\rangle_{\mathrm{max}}$.

In figure 2, we plot the maximum values $\langle\tilde{\chi}^2\rangle_{\mathrm{max}}$ extracted from lattice simulations, as a function of the resonance parameter q_3, and compare them against our theoretical estimation for the critical value $\langle\tilde{\chi}^2\rangle_{\mathrm{crit}}$ in the regime *ii*) with $q_3 \gtrsim 10$, cf. eq. (2.13). Recalling the relation $q_\chi = q_3^2$ we used in our simulations, we can see that the critical variance for $q_3 \gtrsim 10$ decreases inversely proportional to q_3, as $\langle\tilde{\chi}^2\rangle_{\simeq}\langle\tilde{\phi}\rangle/(3q_3)$, hence inversely proportional to the coupling constant σ. Although our analytical prediction eq. (2.13) only captures roughly the real amplitude $\langle\tilde{\chi}^2\rangle_{\mathrm{max}}$,[3] it captures exactly the dependence on q_3.

2.2 Gravitational wave production

In this section, we study GW production during preheating using the recently released module of `CosmoLattice` dedicated to the generation of GWs by scalar fields [137]. The dynamics of

[3] We estimate the maximum variance $\langle\tilde{\chi}^2\rangle_{\mathrm{max}}$ as the average over one period of oscillation of the variance $\langle\tilde{\chi}^2\rangle$, once it has reached its maximum value.

JCAP05(2023)023

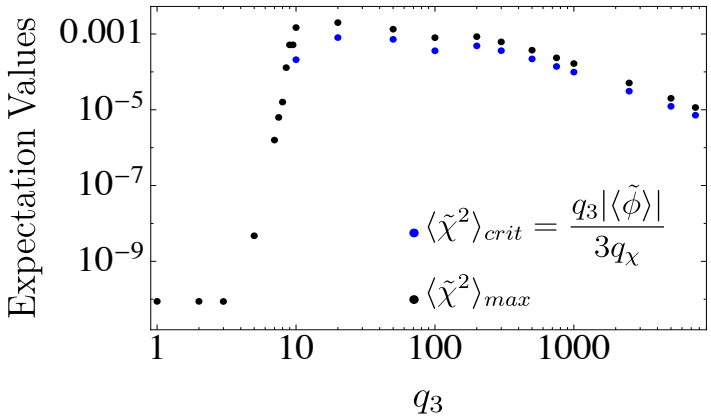

Figure 2. Lattice results of $\langle\tilde{\chi}^2\rangle_{\rm max}$ for different values of q_3 (black dots). It is clearly observed that for $q_3 \lesssim 10$ the amplitude of $\langle\tilde{\chi}^2\rangle_{\rm max}$ is much smaller than for $q_3 \gtrsim 10$, as the tachyonic growth of $\langle\tilde{\chi}^2\rangle$ is simply stopped by the condition $q_{3,\rm eff} = 1/3$. We choose $\langle\tilde{\chi}^2\rangle_{\rm max}$ as the value of $\langle\tilde{\chi}^2\rangle$ averaged over one oscillation when it reaches its maximum value. For comparison, we also show the corresponding theoretical prediction for $q_3 \gtrsim 10$ in eq. (2.13) (blue dots).

GWs are governed by the linearized equation of motion of the tensor perturbations h_{ij},

$$\ddot{h}_{ij} + 3H\dot{h}_{ij} - \frac{\nabla^2}{a^2}h_{ij} = \frac{2}{m_p^2 a^2}\Pi_{ij}^{TT}\,, \tag{2.14}$$

which satisfy $h_{ii} = \partial_i h_{ij} = 0$. Here Π_{ij}^{TT} is the transverse-traceless part of an effective anisotropic stress tensor $\Pi_{ij} = \{\partial_i\phi\partial_j\phi + \partial_i\chi\partial_j\chi\}$. In momentum space, the TT operation is defined as $\Pi_{ij}^{TT}(\mathbf{k},t) = \Lambda_{ijkl}(\mathbf{k})\Pi_{ij}(\mathbf{k},t)$, with the projector Λ defined as

$$\Lambda_{ij,lm}(\hat{\mathbf{k}}) \equiv P_{il}(\hat{\mathbf{k}})P_{jm}(\hat{\mathbf{k}}) - \frac{1}{2}P_{ij}(\hat{\mathbf{k}})P_{lm}(\hat{\mathbf{k}})\,, \qquad P_{ij} = \delta_{ij} - \hat{\mathbf{k}}_i\hat{\mathbf{k}}_j\,, \quad \hat{\mathbf{k}}_i = \mathbf{k}_i/k\,. \tag{2.15}$$

The energy density power spectrum of GWs normalized by the critical energy density of the universe is

$$\Omega_{\rm GW}(k,t) = \frac{1}{\rho_c}\frac{d\rho_{\rm GW}}{d\log k}(\mathbf{k},t) = \frac{k^3}{(4\pi)^3 GV}\int\frac{d\Omega_k}{4\pi}\dot{h}_{ij}(\mathbf{k},t)\dot{h}_{ij}^*(\mathbf{k},t)\,, \tag{2.16}$$

where $d\Omega_k$ represents a solid angle element in $\mathbf{k}$-space. Lattice simulations follow the procedure described in ref. [92], by solving a discrete version of eq. (2.14) (see appendix A for further details). In order to compute the GW energy density power spectrum we make use of a discrete version of eq. (2.16). To obtain the total energy density of GWs, we integrate eq. (2.16) over momentum k,

$$\Omega_{\rm GW}^{\rm tot}(t) = \int d\log k\,\frac{1}{\rho_c}\frac{d\rho_{\rm GW}}{d\log k}(\mathbf{k},t). \tag{2.17}$$

In figure 3, we show in the *Top* panels the matter power spectrum of the daughter field, $\mathcal{P}_{\tilde{\chi}}$, whereas in the *Bottom* panels we show the normalised GW energy density power spectrum $\Omega_{\rm GW}$, as a function of $\kappa = k/m_\phi$. Spectra are measured every $\Delta(m_\phi t) = 0.2$ steps up to a final time $m_\phi t_{\rm f} = 400$, assuring that the system has reached a steady state and the transfer of energy between ϕ and χ fields is negligible. The GWs are produced in pulses coinciding with the periods of tachyonic instability of χ, with step-like jumps visible in both the matter

JCAP05(2023)023

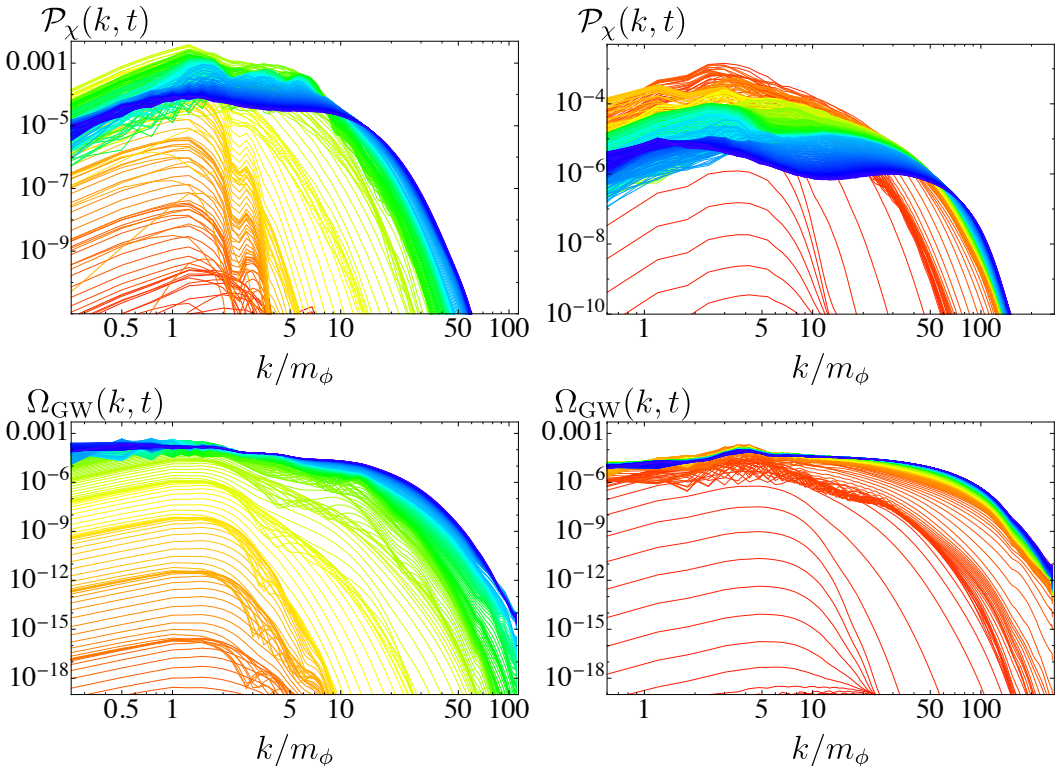

Figure 3. *Top* panels: Matter power spectrum of the daughter field χ, $\mathcal{P}_\chi(k)$, as a function of the momentum k/m_ϕ for $q_3 = 10$ (*Left*) and for $q_3 = 100$ (*Right*). *Bottom* panels: GW energy density power spectrum $\Omega_{\rm GW}(k)$, for $q_3 = 10$ (*Left*) and for $q_3 = 100$ (*Right*). In all panels, colors run from red (early times) to blue (late times). Each spectra is measured every $\Delta(m_\phi t) = 0.2$.

spectra $\mathcal{P}_{\tilde{\chi}}(k,t)$ and in $\Omega_{\rm GW}(k,t)$. The production of GWs ceases when the variance of the daughter field stops growing due to the end of tachyonic resonance (from that moment onward the χ_k modes are no longer excited, so the spatial gradients of $\tilde{\chi}$ do not evolve any further). In figure 4 we show the evolution of the total GW energy density in time. We observe that it grows exponentially until it saturates to a certain value. The saturation occurs of course when $\langle\tilde{\chi}^2\rangle$ stops growing and reaches its maximum value $\langle\tilde{\chi}^2\rangle_{\rm max}$. For instance, we see that GW production for $q_3 = 50$ stops around $m_\phi t \sim 15$, and looking into the *Right* panel of figure 1 we observe that $\langle\tilde{\chi}^2\rangle$ stopped increasing around the same time. Once the GW spectrum saturates, the SGWB redshifts freely. Since the maximum value of $\langle\tilde{\chi}^2\rangle$ depends on q_3, the same dependence is inherited in the maximum value of the GW energy density, see figure 4. Another feature worth noticing is that for $q_3 \gtrsim 10$, the final GW energy density ratio $\Omega^{\rm tot}_{\rm GW}(t)$ reaches a maximum (approximately) fixed amplitude, which can be as high as $\Omega^{\rm tot}_{\rm GW}(t_{\rm f}) \simeq 5 \cdot 10^{-4}$ for $q_3 \simeq 10$, while it decreases smoothly for larger values of q_3 [see eq. (2.22) for a parametrization on the q_3 dependence of the peak amplitude of the SGWB].

The SGWB produced during preheating is redshifted freely once its amplitude saturates. Today's amplitude and peak frequency of the SGWB depend on the expansion history of the universe, so in order to estimate them, we need to redshift the background from the final time of our simulations $t_{\rm f}$, till the present time t_0. This requires to know the expansion history from $t_{\rm f}$ till the moment $t_{\rm RD}$ when radiation domination (RD) is fully established. If we parametrize such intermediate era with an effective equation of state $\bar{w} = p/\rho$, we can

JCAP05(2023)023

write the redshifted frequency and amplitude today of the SGWB as (see appendix B for further details)

$$f_{\rm GW} \simeq 4\times 10^{10}\,\epsilon_{\rm f}^{1/4}\,\frac{k_{\rm GW}}{a_{\rm f}H_{\rm f}}\left(\frac{H_{\rm f}}{m_p}\right)^{1/2}\quad {\rm Hz}\,, \tag{2.18}$$

$$h_0^2\Omega_{\rm GW}^{(0)} \simeq 1.6\times 10^{-5}\,\epsilon_{\rm f}\,\Omega_{\rm GW}^{(\rm f)}\,, \tag{2.19}$$

where $\epsilon_{\rm f}$ is defined as

$$\epsilon_{\rm f} \equiv \left(\frac{a_{\rm f}}{a_{\rm RD}}\right)^{1-3\bar{w}}\,, \tag{2.20}$$

with $a_{\rm f}\equiv a(t_{\rm f})$ and $a_{\rm RD}\equiv a(t_{\rm RD})$. In order to estimate $h_0^2\Omega_{\rm GW}^{(0)}$ and $f_{\rm GW}$ we have characterized the position $\kappa_{\rm p}$ and the amplitude $\Omega_{\rm GW}^{(\rm f)}$ of the peak in the GW spectra at $t_{\rm f}$. While the position of the peak is characterized by the initial instability tachyonic band given in eq. (2.12), the final amplitude of the peak $\Omega_{\rm GW}^{(\rm f)}$ decreases smoothly with the resonance parameter. We have also measured the values of $a_{\rm f}$ and $H_{\rm f}$ in our simulations. Very importantly, we have observed that for $q_3\gtrsim 10$ the dominant contribution to the total energy of the system comes from the daughter field, which behaves as radiation. Therefore, the system at $t_{\rm f}$ is already quite close to RD, with an equation of state $\bar{\omega}$ slightly smaller than (but very close to) $\bar{\omega}\simeq 1/3$. This implies that we can estimate $\epsilon_{\rm f}$ to be $\lesssim 1$. Putting everything together and taking $\epsilon_{\rm f}=1$ for simplicity, we find the following parametrization for the SGWB peak today (valid only for $q_3\gtrsim 9$)

$$f_{\rm GW}^{(p,0)}(q_3) \simeq (1.4\pm 0.1)\times 10^{8}\,\left(\frac{q_3}{10}\right)^{0.53\pm 0.03}\quad {\rm Hz}\,, \tag{2.21}$$

$$h_0^2\Omega_{\rm GW}^{(p,0)}(q_3) \simeq (4.9\pm 1.6)\times 10^{-9}\,\left(\frac{q_3}{10}\right)^{-0.63\pm 0.14}\,. \tag{2.22}$$

We observe that the produced SGWB has a rather large amplitude but is peaked at high frequencies. We also note that the exponent of our frequency characterization coincides with that in eq. (2.12). While a high-frequency detection program at $\sim$ MHz frequencies and above, has been recently put forward [138], this is yet in its infancy, and the reality of the situation is that neither current nor planned GW detection experiments are so far expected to be able to detect these high frequency SGWBs. Direct detection is therefore challenging, as it is also usually the case in $\phi^2\chi^2$ preheating scenarios with monomial inflaton potentials.

As the GW production is in any case very significant in our scenario, we may still look for another manner to probe these backgrounds, namely, using indirect constraining means. In particular, as GWs produced during preheating have shorter wavelengths than the Hubble scale at the time of production, they contribute to the energy density of the universe as radiation [112]. Hence, it might be possible to set bounds on the amount of GW energy density that can be produced, by using cosmological constraints on the total radiation density species allowed in the universe. This is typically parameterized by a deviation of the effective number of relativistic degrees of freedom beyond the Standard Model $\Delta N_{\rm eff}=N_{\rm eff}-N_{\rm eff,SM}$, with $N_{\rm eff,SM}=3.0440$ [139]. Assuming that only our SGWB contributes to the extra radiation energy density at the time of CMB decoupling, a bound on the extra radiation degrees of freedom $\Delta N_{\rm eff}$ sets a constraint on $h_0^2\Omega_{\rm GW}^{(0)}$ as [112]

$$\frac{h_0^2\Omega_{\rm GW}^{(0)}}{h_0^2\Omega_{\gamma}^{(0)}} = \frac{7}{8}\left(\frac{4}{11}\right)^{4/3}\Delta N_{\rm eff}\,, \tag{2.23}$$

JCAP05(2023)023

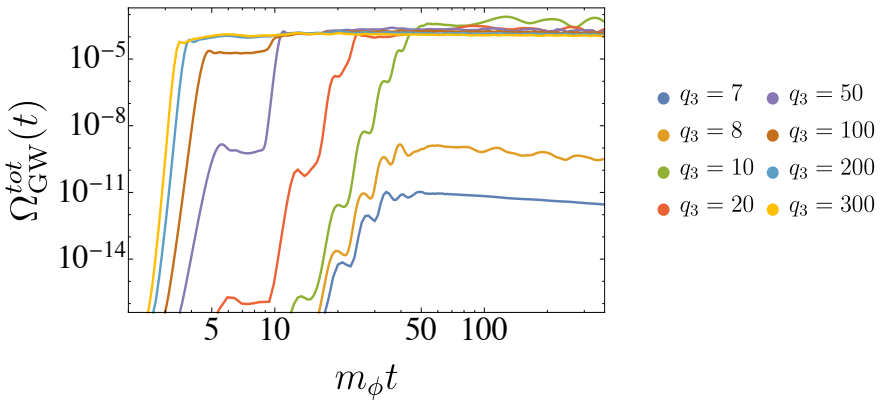

Figure 4. Time evolution of the GW total energy density for different values of q_3.

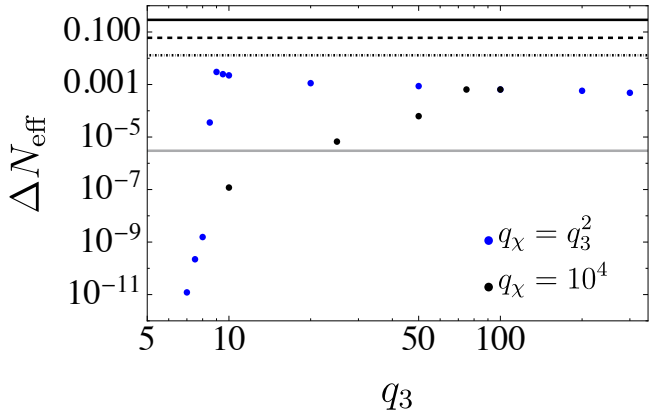

Figure 5. Number of relativistic degrees of freedom beyond Standard Model for different values of q_3, for the relation $q_\chi = q_3^2$ and fixed $q_\chi = 10^4$. The solid top line corresponds to the current Planck bound $\Delta N_{\rm eff} \lesssim 0.29$, whereas the dashed line below represents the future CMB-S4 $\Delta N_{\rm eff} \lesssim 0.06$ upper bound at 2σ. The dash-dotted line corresponds to the upper bound imposed by next generation satellite missions at 2σ, $\Delta N_{\rm eff} \lesssim 0.013$. The gray bottom solid line corresponds to a hypothetical cosmic variance limited (CVL) CMB polarization experiment upper bound $\Delta N_{\rm eff} \lesssim 3 \cdot 10^{-6}$.

where the present energy density of photons is $h_0^2 \Omega_\gamma^{(0)} = 2.47 \times 10^{-5}$. The Planck observations set a limit $|\Delta N_{\rm eff}| \lesssim 0.29$ at 95% C.L. [127, 128], whereas the next-generation CMB-S4 experiments will probe $\Delta N_{\rm eff} \lesssim 0.06$ at 2σ [129]. Additionally, the next generation of satellite missions like COrE [130] and Euclid [131] will impose bounds at 2σ on $\Delta N_{\rm eff} \lesssim 0.013$. A hypothetical cosmic variance limited (CVL) CMB polarization experiment could presumably get down to $\Delta N_{\rm eff} \lesssim 3 \cdot 10^{-6}$ [140], though this does not seem experimentally realistic. In figure 5, we show $\Delta N_{\rm eff}$ for different values of q_3 considering two cases: $q_\chi = q_3^2$ (blue dots) and $q_\chi = 10^4$ (black dots). We found that the coupling that produces the largest amount of GWs is $q_3 = 9$, yielding $\Delta N_{\rm eff} \simeq 0.003$, which is above the bound expected in a hypothetical CVL experiment, but still below the sensitivity of actually planned realistic experiments.

We conclude therefore that neither direct or indirect detection methods can probe the SGWBs predicted in the scenario studied in this section, as either the peak frequency of the GW signals is too high, or the amount of GW energy density produced is simply not

JCAP05(2023)023

enough to be constrained by $\Delta N_{\rm eff}$. In order to improve this situation, two circumstances could be sought for: 1) decreasing the energy scale of inflation, so that we can shift to smaller frequencies the SGWB peak, and/or 2) increasing the amount of GWs produced relative to the field energy budget in the universe. In the next section, we introduce a polynomial potential for the inflaton which, *a priori*, seems to allow to satisfy both conditions. We therefore explore next the extent to which GW production during preheating after polynomial inflation can improve the detectability of the SGWB due to a trilinear interaction.

3 Polynomial potential

In this section, we consider the most general renormalizable single-field model of inflation, where the inflaton potential is a polynomial of degree four [141]

$$\begin{aligned} V_{\rm inf}\left(\phi\right) &= \frac{1}{2}m_\phi^2\phi^2 + \sigma_\phi\phi^3 + \lambda_\phi\phi^4 \\ &= \lambda_\phi\left(2\,\phi_0^2\,\phi^2 - \frac{8}{3}\,(1-\beta)\,\phi_0\phi^3 + \phi^4\right), \end{aligned} \tag{3.1}$$

where in the second line we have parametrized the mass and trilinear coupling of the inflaton as $m_\phi \equiv 2\sqrt{\lambda_\phi}\phi_0$ and $\sigma_\phi \equiv -\frac{8}{3}\lambda_\phi(1-\beta)\phi_0$. The linear term in ϕ is absent in the potential of eq. (3.1) since it can be absorbed by shifting the field, whereas a constant term is ignored since we set it to equal to the value of the cosmological constant today, which is negligible compared to the energy scale of inflation [141]. All three terms in eq. (3.1) are used to match the observational data, and the existence of a (near) inflection-point at ϕ_0 guarantees the flatness of the polynomial potential of quartic order. In this setup, λ_ϕ is the inflaton self-coupling, and β is a parameter that controls the flatness configuration in the vicinity of ϕ_0. Notice that, if $\beta < 0$, there is a false vacuum for $\phi > \phi_0$, and the inflaton can get stuck in this second minimum [142]. Hence, in this work, we focus on the case where $0 < \beta \ll 1$, and on small inflaton amplitudes, so that the inflaton field value is sub-Planckian at the time when the curvature perturbations observed at the CMB are generated, i.e., we will assume $\phi_0 \leq m_p$ [141, 142]. Interestingly, the inflection-point ϕ_0 constitutes the only free parameter in this inflationary model, since all the couplings in the potential eq. (3.1) can be expressed at its expense (for more details of this, see refs. [141, 142]). In particular, by considering the CMB measurements from Planck data [1] on the scalar power spectrum $P_\zeta = (2.1 \pm 0.1) \times 10^{-9}$, and on the spectral index $n_s = 0.9649 \pm 0.0042$, and assuming these were generated $N_e = 65$ e-folds before the end of inflation, the quantities λ_ϕ, β and m_ϕ^2, can be fixed as

$$\lambda_\phi \simeq 6.61 \times 10^{-16}\left(\frac{\phi_0}{\rm m_p}\right)^2, \tag{3.2}$$

$$\beta \simeq 9.73 \times 10^{-7}\left(\frac{\phi_0}{\rm m_p}\right)^4, \tag{3.3}$$

$$m_\phi = 2\,\sqrt{\lambda_\phi}\,\phi_0 \simeq 5 \times 10^{-8}\left(\frac{\phi_0}{m_p}\right)^2 m_p\,. \tag{3.4}$$

As a lower bound $\phi_0 \geq 3 \times 10^{-5} m_p$ emerges naturally by demanding the stability of the inflationary scenario against radiative corrections [141, 142], the inflection point ϕ_0 ranges in

JCAP05(2023)023

practice within the interval $3 \times 10^{-5} m_p < \phi_0 \leq m_p$. The inflaton mass lies therefore in our modeling within the range $10^2\,\mathrm{GeV} < m_\phi \leq 10^{11}\,\mathrm{GeV}$.

The full potential of the system inflaton-daughter field is then again

$$V(\phi, \chi) = V_{\mathrm{inf}}(\phi) + \frac{\sigma}{2}\,\phi\,\chi^2 + \frac{\lambda}{4}\,\chi^4\,, \tag{3.5}$$

and in order to ensure that this potential is bounded from below, we require $\lambda_\phi, \lambda > 0$. Identifying a critical value for the self-coupling of χ as

$$\lambda_c(\sigma, \lambda_\phi, \phi_0) \equiv \frac{\sigma^2}{8\,\lambda_\phi\,\phi_0^2}\,. \tag{3.6}$$

We observe that for $0 < \lambda < \lambda_c$, the potential (3.5) has two minima at non-vanishing values of χ and ϕ, where the potential is negative, $V(\phi, \chi) < 0$. For $\lambda \geq \lambda_c$ instead, there is only one minimum at $\phi = \chi = 0$ with $V(\phi, \chi) = 0$. In the following analysis we use the limiting case $\lambda = \lambda_c$, as this value corresponds, as we will see, to the case for which the production of GWs is maximized.

3.1 Preheating dynamics. Lattice simulations

Similarly to the case of the monomial potential, we can perform a change of variables such that we are able to write the equations of motion with dimensionless quantities. We choose conveniently

$$d\tilde{x}^\mu = \sqrt{\lambda_\phi}\,\phi_0\,dx^\mu\,, \quad \tilde{\phi} = \frac{\phi}{\phi_0}\,, \quad \tilde{\chi} = \frac{\chi}{\phi_0}\,, \quad \tilde{H} = \frac{H}{\sqrt{\lambda_\phi}\phi_0}\,, \tag{3.7}$$

such that the equations of motion for ϕ and χ become

$$\tilde{\phi}'' + 3\,\tilde{H}\,\tilde{\phi}' + 4\,\tilde{\phi} - 8\,(1-\beta)\,\tilde{\phi}^2 + 4\,\tilde{\phi}^3 + \frac{q_3}{2}\,\tilde{\chi}^2 - \frac{\tilde{\nabla}^2\tilde{\phi}}{a^2} = 0\,, \tag{3.8}$$

$$\tilde{\chi}'' + 3\,\tilde{H}\,\tilde{\chi}' + q_3\,\tilde{\chi}\,\tilde{\phi} + q_\chi\,\tilde{\chi}^3 - \frac{\tilde{\nabla}^2\tilde{\chi}}{a^2} = 0\,, \tag{3.9}$$

where $'$ denotes derivatives with respect to the new time variable. The resonance parameters emerging now in the problem are defined as

$$q_3 \equiv \frac{\sigma}{\lambda_\phi\,\phi_0} \quad \text{and} \quad q_\chi \equiv \frac{\lambda}{\lambda_\phi}\,. \tag{3.10}$$

A relation between q_χ and q_3, equivalent to $\lambda \geq \lambda_c$, so that there is only one minimum at $\tilde{\phi} = \tilde{\chi} = 0$ where $V\left(\tilde{\phi}, \tilde{\chi}\right) = 0$, can be obtained as

$$q_\chi > \frac{q_3^2}{8}\,. \tag{3.11}$$

Introducing the field decomposition from eq. (2.6) into eq. (3.9), and using again the Hartree approximation $\tilde{\chi}^3 \to 3\,\tilde{\chi}\,\langle\tilde{\chi}^2\rangle$, we find that the mode functions of $\tilde{\chi}$ obey

$$\tilde{\chi}_k'' + 3\,\tilde{H}\tilde{\chi}_k' + \left(3\,q_\chi\,\left\langle\tilde{\chi}^2\right\rangle + q_3\,\tilde{\phi}\,(t) + \frac{\kappa^2}{a^2}\right)\tilde{\chi}_k = 0\,, \quad \text{where} \quad \kappa \equiv \frac{k}{\sqrt{\lambda_\phi}\phi_0} \tag{3.12}$$

ϕ_0	$\tilde{\phi}(t_i)$	$\tilde{\phi}'(t_i)$
m_p	0.368	-0.395
$10^{-1}\, m_p$	0.473	-0.464
$10^{-2}\, m_p$	0.485	-0.470
$10^{-3}\, m_p$	0.486	-0.471

Table 1. The initial amplitude and velocity of the inflaton for different values of ϕ_0.

The χ field has therefore an effective time-dependent mass $m_{\tilde{\chi}}^2 \approx \left(q_3\, \tilde{\phi}\,(t) + 3q_\chi \langle \tilde{\chi}^2 \rangle\right)$, which oscillates between negative and positive values due to the oscillations of the inflaton. Whenever $m_{\tilde{\chi}}^2 < 0$ and $\kappa^2/a^2 < -m_{\tilde{\chi}}^2$, the mode frequency $\tilde{\omega}_k^2 \equiv \kappa^2/a^2 + m_{\tilde{\chi}}^2$ will become negative leading to an exponential growth of the corresponding $\tilde{\chi}_k$ modes. The power spectrum of the excited modes $\mathcal{P}_{\tilde{\chi}}(k,t)$, and consequently the variance of the daughter field $\langle \tilde{\chi}^2 \rangle$, will then grow exponentially in a step-like manner, every time the inflaton amplitude turns negative.

In order to follow in detail the dynamics of tachyonic resonance in this scenario, similarly as in section 2.1, we have considered eqs. (3.8) and (3.9) and solved numerically a discrete version of these. We obtain the initial amplitude and velocity of the inflaton from the breaking of the slow-roll condition when $\epsilon_H = 1$, for different values of ϕ_0, see table 1. The initial condition for the χ field is again set to an initially vanishing homogeneous amplitude, on top of which we add quantum vacuum fluctuations, following the standard recipe for initial lattice power spectra (see e.g. section 7 of ref. [135] for details)

We have performed a series of lattice simulations with $N = 512$ sites per dimension and a minimum infrared momentum $\kappa_{\rm IR} \in [0.5 : 6]$, making sure we capture well all relevant scales. Simulations were run for different values of q_3 considering the relation $q_\chi = q_3^2/8$ for $q_3 \in [25 : 5 \times 10^4]$, finishing at $\sqrt{\lambda_\phi}\phi_0 t_{\rm f} = 400$, as this guarantees that the system has reached a steady state.

The dynamics of preheating in the polynomial scenario can be described as follows. In an initial stage, the inflaton oscillates around its minimum, like in the monomial scenario, except that the nature of the potential of eq. (3.1) makes the first oscillations to be an-harmonic. As the amplitude decays with the expansion of the universe, the oscillations become gradually more and more harmonic, as the potential becomes essentially more and more quadratic around the minimum. As within each oscillation the inflaton becomes negative during half of the oscillation, the effective mass $m_{\tilde{\chi}}$ of the $\tilde{\chi}_k$ modes becomes also negative for $\kappa < \sqrt{\sigma|\phi|}\, a$. This induces an exponential growth of such IR modes during the semi oscillations with $\phi < 0$, as can be clearly observed in figure 6. As in the previous scenario we identify two regimes depending on the value of q_3:

i) For $q_3 \lesssim 100$, tachyonic resonance ends due to the expansion of the universe, since the effective resonance parameter $q_{3,\rm eff} = q_3|\langle\tilde{\phi}\rangle|$ decreases with the scale factor. When $q_{3,\rm eff} < 1$ is achieved, the system enters into a narrow regime where tachyonic resonance is not efficient anymore. This can be observed clearly in the *Left* panel of figure 6.

ii) For $q_3 \gtrsim 100$, tachyonic resonance rather ends (before it becomes narrow) due to the presence of the self-interaction of the χ field. This happens when the χ self-interaction term in $m_{\tilde{\chi}}^2$ overtakes the trilinear interaction term. In that moment the variance $\langle \tilde{\chi}^2 \rangle$

JCAP05(2023)023

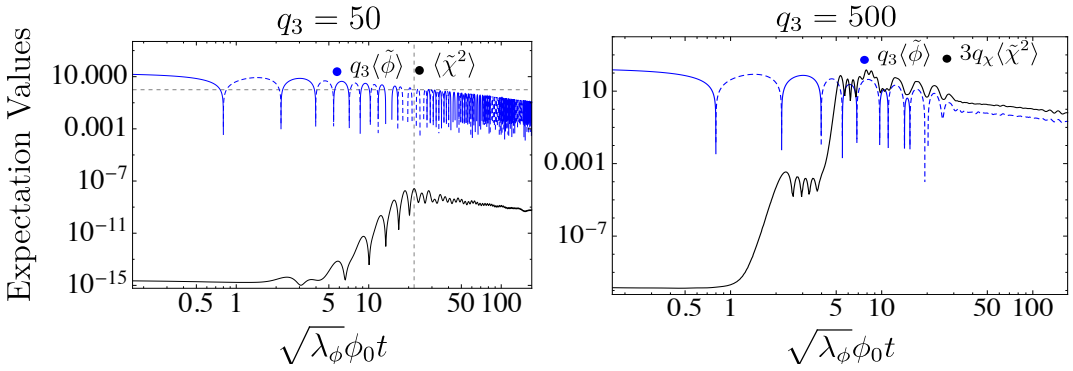

Figure 6. *Left*: Time evolution of the inflaton's volume average $\langle\tilde{\phi}\rangle$ times the resonance parameter q_3 ($q_{3,\text{eff}}$), and the variance of the daughter field $\langle\tilde{\chi}^2\rangle$ for $q_3 = 50$. The horizontal dashed line represents $q_{3,\text{eff}} = 1$, whereas the vertical dashed line is the time at which the maximum value of the variance, $\langle\tilde{\chi}^2\rangle_{\text{max}}$, is reached. *Right*: Time evolution of $q_3\langle\tilde{\phi}\rangle$ and the variance of the daughter field $\langle\tilde{\chi}^2\rangle$ times $3\,q_\chi$ for $q_3 = 500$. We see that once the term $3q_\chi\langle\tilde{\chi}^2\rangle$ overtakes $q_3\langle\tilde{\phi}\rangle$ the growth of the variance stops. For both panels, the solid (dashed) blue lines are the positive (negative) part of the inflaton mean value.

reaches a maximal critical value, which can be expressed as

$$\left\langle\tilde{\chi}^2\right\rangle_{\text{crit}} \simeq \frac{q_3|\langle\tilde{\phi}\rangle|}{3\,q_\chi}\,. \tag{3.13}$$

The end of tachyonic resonance when $\langle\tilde{\chi}^2\rangle$ reaches its critical value (3.13) can be observed in the *Right* panel of figure 6.

In figure 7, we show the theoretical prediction for $q_3 \gtrsim 100$ of the maximum value of $\langle\tilde{\chi}^2\rangle$ given by eq. (3.13) (blue dots), together with the actual values obtained in our lattice simulations (black dots). We observe that for $q_3 \lesssim 100$ the variance $\langle\tilde{\chi}^2\rangle$ grows with q_3, while for $q_3 \gtrsim 100$ it decays inversely proportional to q_3, in correspondence with the theoretical description $\langle\tilde{\chi}^2\rangle_{\text{crit}} \simeq \frac{q_3\langle\tilde{\phi}\rangle}{3\,q_\chi} = \frac{8\langle\tilde{\phi}\rangle}{3\,q_3}$ [in the last identity we have introduced the saturation relation $q_\chi = \frac{q_3^2}{8}$ from eq. (3.11)]. While our theoretical estimation in eq. (3.13) captures only approximately the truly measured maximum variance $\langle\tilde{\chi}^2\rangle_{\text{max}}$ for $q_3 \gtrsim 100$, it describes nonetheless exactly its dependence on q_3. In such regime, after the variance reaches the critical value $\langle\tilde{\chi}^2\rangle_{\text{max}} \simeq \langle\tilde{\chi}^2\rangle_{\text{crit}}$, the system dynamics become fully non-linear in the following stages, due to the backreaction of the daughter field into the inflaton. Similarly as in the scenario with the monomial potential, due to the non-zero value acquired by the variance of χ, the inflaton is forced to oscillate around a new minimum developed in its effective potential, a minimum that corresponds to a negative value of ϕ.

3.2 Gravitational wave production

In this section, we study the production of GWs during preheating after polynomial inflation. We follow the same procedure explained in section 2.2, tracking the real time dynamics of the GWs and measuring their energy density power spectrum $\Omega_{\text{GW}}(k,t)$, cf. eq. (2.16). In figure 8, we show $\Omega_{\text{GW}}(k,t)$ and the matter power spectrum of the daughter field $\mathcal{P}_{\tilde{\chi}}(k)$. Spectra are measured every $\Delta(\sqrt{\lambda_\phi}\phi_0 t) = 0.2$ intervals, up to a final time $\sqrt{\lambda_\phi}\phi_0 t_{\text{f}} = 400$. We see that GWs are produced in pulses coinciding with the growth of the variance $\langle\tilde{\chi}^2\rangle$ of the daughter

JCAP05(2023)023

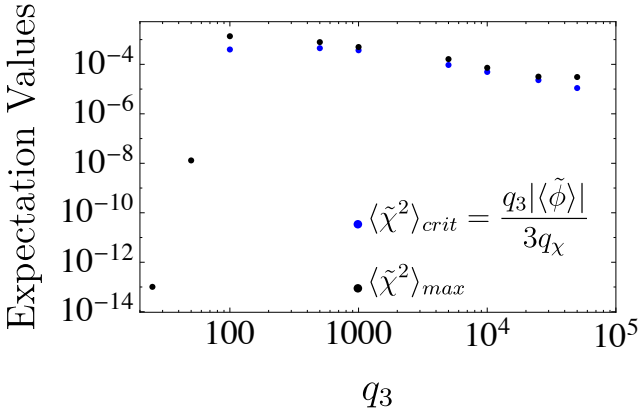

Figure 7. Lattice results of $\langle\tilde{\chi}^2\rangle_{\rm max}$ for different values of q_3 (black dots). It is clearly observed that for $q_3 \lesssim 100$ the amplitude of $\langle\tilde{\chi}^2\rangle_{\rm max}$ is much smaller than for $q_3 \gtrsim 100$, as the tachyonic growth of $\langle\tilde{\chi}^2\rangle$ is simply stopped by the condition $q_{3,\rm eff} = 1$. We choose $\langle\tilde{\chi}^2\rangle_{\rm max}$ as the value of $\langle\tilde{\chi}^2\rangle$ averaged over one oscillation when it reaches its maximum value. For comparison we also show the corresponding theoretical prediction for $q_3 \gtrsim 100$ in eq. (3.13) (blue dots).

field. The production of GWs in the regime $q_3 \gtrsim 100$, stops around the time when $\langle\tilde{\chi}^2\rangle$ reaches its maximum critical value $\langle\tilde{\chi}^2\rangle_{\rm crit}$. At this moment, the growth of $\Omega_{\rm GW}(k,t)$ ceases and the non-linearities developed in the dynamics of the inflaton-daughter system leads to a transfer of power into more ultraviolet (UV) modes in the GW spectrum.

Fixing $q_\chi = q_3^2/8$ according to the saturation relation, we have characterized the amplitude and the peak position of the GW background as a function of ϕ_0 and q_3. In the *Left* panel of figure 9, we plot the time evolution of the GW total energy density for different values of ϕ_0, and observe that the total GW energy density decreases with ϕ_0. On the other hand, decreasing ϕ_0 implies decreasing the energy scale of inflation, and hence also the peak frequency of the signal today $f_{\rm GW}^{(p,0)}$. In the *Right* panel of figure 9, we plot the time evolution of the GW total energy density for different values of q_3, and observe that the final amplitude decreases mildly when increasing this parameter. At the same time, the dependence of $f_{\rm GW}^{(p,0)}$ on the resonance parameter q_3 is determined by the initial instability band, $\kappa^2 < q_3|\dot{\phi}|\,a$. Regarding the expansion history of the universe, which is relevant for the determination the $\epsilon_{\rm f}$ parameter to redshift correctly the signal, our lattice simulations indicate that for sufficiently large couplings $q_3 \gtrsim 10^3$ the energy budget of the system is dominated by kinetic and gradient energy of the daughter field, which behaves as radiation. The universe is therefore in RD when we end our simulations, and therefore we take $\epsilon_{\rm f} = 1$. Using eqs. (2.18) and (2.19), we obtain a parametrization of the SGWB's peak position and amplitude, as function of ϕ_0 and q_3, valid for $q_3 \gtrsim 10^3$ and $3\times10^{-5}m_p \leq \phi_0 \leq m_p$, as

$$f_{\rm GW}^{(p,0)}(\phi_0,q_3) \simeq (5.05\pm2.03)\times10^6 \left(\frac{\phi_0}{m_p}\right)^{0.31\pm0.1}\left(\frac{q_3}{100}\right)^{0.4\pm0.06}\ {\rm Hz}\,, \tag{3.14}$$

$$h_0^2\Omega_{\rm GW}^{(p,0)}(\phi_0,q_3) \simeq (4.5\pm4)\times10^{-9}\left(\frac{\phi_0}{m_p}\right)^{1.41\pm0.13}\left(\frac{q_3}{100}\right)^{-0.75\pm0.12}\,. \tag{3.15}$$

From the parametrization we observe that the maximum amplitude for the SGWB is obtained for $\phi_0 \simeq m_p$, but in that case the background is peaked at very high frequencies $f_{\rm GW}^{(p,0)} \gtrsim 5\cdot10^6$

JCAP05(2023)023

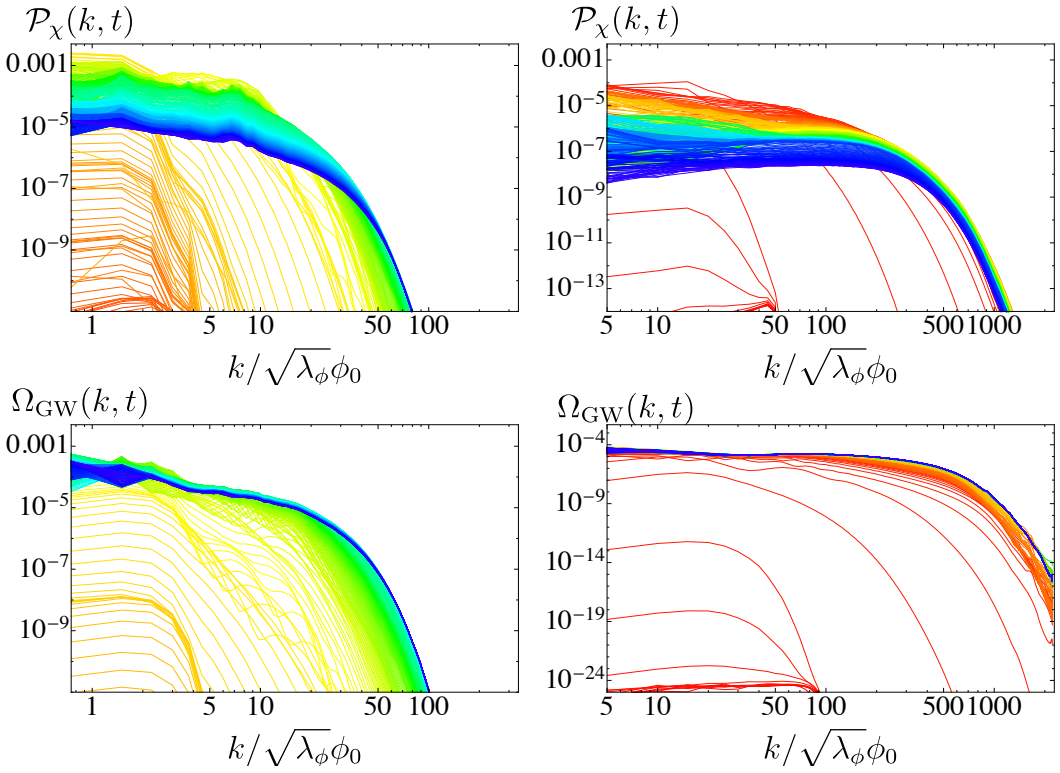

Figure 8. *Top* panels: Matter power spectrum of the daughter field $\mathcal{P}_{\tilde{\chi}}(k,t)$, as a function of the momentum k/m_ϕ for $q_3 = 100$ (*Left*) and for $q_3 = 10^4$ (*Right*). *Bottom* panels: GW energy density power spectrum $\Omega_{\rm GW}(k,t)$, for $q_3 = 100$ (*Left*) and for $q_3 = 10^4$ (*Right*). In all panels, colors run from red in early times to blue in late times. Spectra are measured every $\Delta(\sqrt{\lambda_\phi}\phi_0 t) = 0.2$ until saturation.

Hz. While decreasing ϕ_0 allow us to move the frequency window to smaller values, down to values $f_{\rm GW}(\phi_0 = 3\cdot 10^{-5}\, m_p) \sim 10^5$ Hz, this can only be done at the expense of suppressing the amplitude of the SGWB spectrum, which then becomes $h_o^2\Omega^{(0)}_{\rm GW}(\phi_0 = 10^{-5}\, m_p) \lesssim 10^{-15}$. Furthermore, the dependence on the resonance parameter q_3 just follows a similar behavior as in parametric resonance [97], so that increasing q_3 parametrically shifts the signal to higher frequencies while decreasing its amplitude.

In conclusion, despite the fact that in the polynomial modeling we achieve partially our intention of shifting to smaller frequencies the SGWB, this can only be done at the expense of suppressing the amplitude of the signal. In order to have a large amplitude background we are forced to have it peaked, as usual, at very high frequencies, where direct detection experiments are yet far from the desired capabilities of detection. Given the inability to detect the SGWB directly also in this model, we can still see whether constraints on a maximum trilinear interaction coupling could be placed using current and planned constraints on $\Delta N_{\rm eff}$. Recalling eq. (2.23), we translate the energy density of the GW background into $\Delta N_{\rm eff}$ and compare with the present/projected bounds on $\Delta N_{\rm eff}$, as we can see in figure 10. We find that for $q_3 = 100$ and $\phi_0 = m_p$, we obtain a maximum value as $\Delta N_{\rm eff} \simeq 0.0021$, which is well above a futuristic CVL experiment, but still below the more realistic expected bounds in near future experiments. We conclude therefore that it is not possible to probe directly or indirectly the predicted signal with upcoming experiments.

JCAP05(2023)023

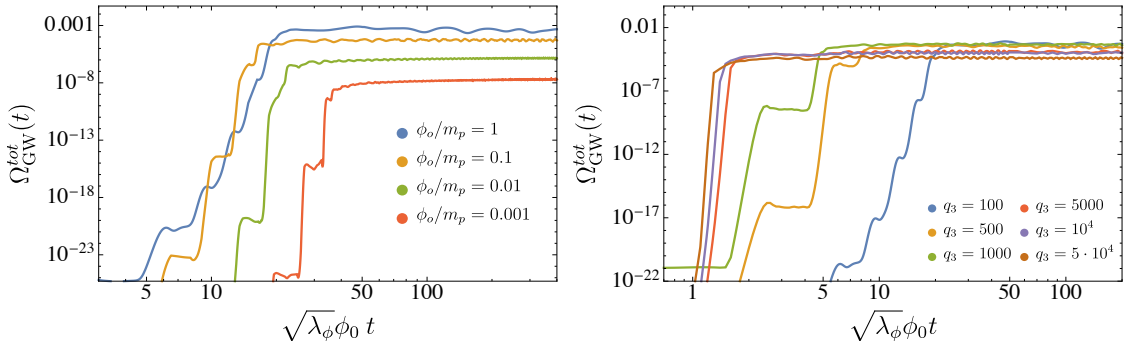

Figure 9. Time evolution of GWs total energy density: *Left:* for different values of ϕ_0, with $q_3 = 100$ and $q_\chi = q_3^2/8$. We observe that the largest amount of GWs is produced by $\phi_0 = m_p$. *Right:* For different values of q_3, with $q_\chi = q_3^2/8$ and $\phi_0 = m_p$.

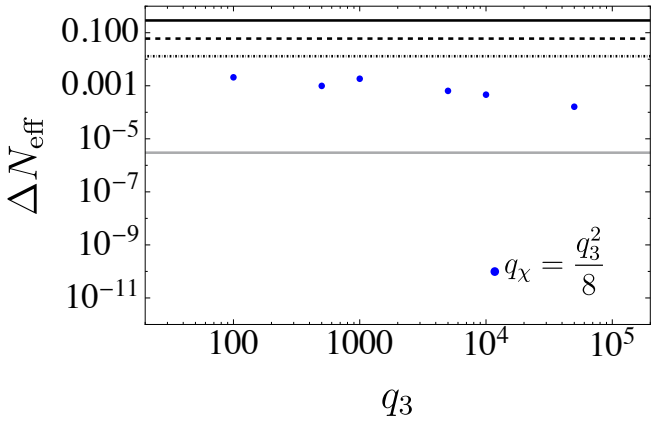

Figure 10. Number of relativistic degrees of freedom beyond Standard Model, $\Delta N_{\rm eff}$, for different values of q_3 with $q_\chi = q_3^2/8$. The top solid black line corresponds to the current bound coming from Planck data $\Delta N_{\rm eff} \lesssim 0.29$, the dashed line below represents the future CMB-S4 $\Delta N_{\rm eff} \lesssim 0.06$ upper bound at 2σ. The dot-dashed black line corresponds the projected bounds at 2σ on $\Delta N_{\rm eff} \lesssim 0.013$ from next-generation satellite missions, whereas the bottom gray solid line corresponds to a hypothetical cosmic variance limited (CVL) CMB polarization experiment upper bound $\Delta N_{\rm eff} \lesssim 3 \cdot 10^{-6}$.

4 Discussion

In this work, we have studied the GW production during preheating due to a trilinear interaction $\phi\chi^2$ between a singlet inflaton ϕ and a daughter scalar field χ. Considering first a preheating scenario with the inflaton having a quadratic monomial potential $\frac{1}{2}m_\phi^2\phi^2$ after inflation, we have added a self-interaction term for the daughter field $\frac{1}{4}\lambda\chi^4$, to ensure the total potential to be bounded from below. This imposes a relation between the resonance parameters q_3 and q_χ, which control the intensity of the daughter field excitation. Only values for which the relation $q_\chi > \frac{q_3^2}{2}$ is satisfied avoid runaway solutions of χ. Using `CosmoLattice` to perform lattice simulations of the system, we find that for $q_3 \lesssim 10$ the growth of the daughter field variance $\langle\tilde{\chi}^2\rangle$ stops at an early moment due to the expansion of the universe, determined by when the system enters into narrow resonance. For $q_3 > 10$ instead, the variance grows up to a critical value $\langle\tilde{\chi}^2\rangle_{\rm crit}$, determined by when the χ self-interaction overtakes the trilinear interaction. GW production follows the step-like growth of the daughter field power spectrum,

JCAP05(2023)023

and ceases once the variance of χ reaches its critical value $\langle\tilde{\chi}^2\rangle_{\rm crit}$, see figures 1 and 4. While the SGWB produced in this preheating scenario can reach an amplitudes as large as $h_0^2\Omega_{\rm GW}^{(0)} \simeq 10^{-9}$, the signal is peaked at high frequencies $f_{\rm GW} \gtrsim 10^8$ Hz, which precludes GW direct detection experiments to detect this background. A large amount of GWs is generated nevertheless in this scenario, which can yield a value in terms of an effective number of relativistic species as large as $\Delta N_{\rm eff} \sim 0.003$ (corresponding to $q_3 = 9$). Unfortunately, this is still below the projected sensitivity on $\Delta N_{\rm eff}$ of next-generation CMB experiments.

We have also studied the case where the inflaton has a polynomial potential (both during preheating and inflation), whose shape is controlled by a single parameter, the value of a near inflection point ϕ_0 in the potential, which can range within $3 \times 10^{-5} m_p < \phi_0 < m_p$. This scenario might improve the situation in two directions: a) decreasing the energy scale of inflation, hence shifting to smaller frequencies the SGWB peak; b) increasing the amount of GW energy density produced relative to the field energy budget of the system. In this scenario, runaway solutions of χ are avoided if the resonance parameters satisfy the relation $q_\chi > \frac{q_3^2}{8}$. Using $\mathcal{C}$osmo$\mathcal{L}$attice to perform lattice simulations of the system, we find that for $q_3 \lesssim 100$, tachyonic resonance ends soon after the onset of inflaton oscillations, when the system enters into narrow resonance due to the expansion of the universe. For $q_3 \gtrsim 100$ instead, tachyonic resonance stops when the variance of the daughter field reaches a critical value $\langle\tilde{\chi}^2\rangle_{\rm crit}$, which occurs when the χ self-interaction term overtakes the trilinear interaction term. Regarding GW production, we find that choosing the highest possible value of the inflection point, $\phi_0 = m_p$, leads to the largest GW production, with a SGWB amplitude as large as $\Omega_{\rm GW}^{(0)} h_0^2 \simeq 5 \cdot 10^{-9}$. This signal is however still peaked at large $f_{\rm GW} \simeq 5 \cdot 10^6$ Hz, which cannot be probed by planned GW experiments. While we can shift the signal down to $\sim 10^5$ Hz frequencies by decreasing ϕ_0 down to its minimum value compatible with CMB constraints, we can only do it at the expense of suppressing the signal amplitude down to $h^2\Omega_{\rm GW}^{(p,0)} \simeq 10^{-15}$. In terms of radiation degrees of freedom represented by the SGWB in this model, we find a maximum value as $\Delta N_{\rm eff} \simeq 0.0021$, which is still out of the reach of near future next-generation CMB experiments.

In summary, preheating scenarios with an inflaton monomial or polynomial potential, and a trilinear coupling between the inflaton and a daughter field, can lead to very efficient GW production. The resulting GW signal is however out of the reach of current and planned direct and indirect probes of SGWBs. One direction we may explore in the future is to consider the same type of coupling in lower scale inflationary scenarios, for which the SGWB frequency peak could be shifted to smaller values, while there is no particular reason to expect the efficiency of GW production to be suppressed.

Acknowledgments

We thank Djuna Croon for interesting discussions and collaboration at early stages of the project. C.C. is also supported by the grant PROMETEO-2019-083, the European Union's Horizon 2020 research and innovation programme under the Marie Skłodowska-Curie grant agreement No 860881-HIDDeN, and partially by the FCT project Grant No. CERN /FIS-PAR/0027/2021. D.G.F. (ORCID 0000-0002-4005-8915) is supported by a Ramón y Cajal contract with Ref. RYC-2017-23493. Our work is supported by the Generalitat Valenciana grant PROMETEO/2021/083, and by the Spanish Ministerio de Ciencia e Innovacion grant PID2020-113644GB-I00. We are also very thankful for the use of computational resources

JCAP05(2023)023

provided by Finis-Terrae II cluster of CESGA (Centro de Supercomputación de Galicia), LluisVives and Tirant clusters of Universitat de València.

A Gravitational wave evolution in the lattice

In order to evolve the h_{ij} fields in the lattice, we follow the method introduced in [92]. We evolve a set of fields u_{ij} with the equation of motion

$$\ddot{u}_{ij} + 3H\dot{u}_{ij} - \frac{\nabla^2}{a^2}u_{ij} = \frac{2}{m_p^2 a^2}\{\partial_i\phi\partial_j\phi + \partial_i\chi\partial_j\chi\}\,. \tag{A.1}$$

The physical h_{ij} tensor perturbations are obtained through

$$h_{ij}(k,t) = \Lambda_{ijkl}(\hat{k})\, u_{kl}(k,t)\,, \tag{A.2}$$

where Λ_{ijkl} is defined by

$$\Lambda_{ijlm}(\hat{\mathbf{k}}) \equiv P_{il}(\hat{\mathbf{k}})P_{jm}(\hat{\mathbf{k}}) - \frac{1}{2}P_{ij}(\hat{\mathbf{k}})P_{lm}(\hat{\mathbf{k}})\,, \tag{A.3}$$

$$P_{ij} = \delta_{ij} - \hat{k}_i\hat{k}_j\,, \quad \hat{k}_i = k_i/k\,. \tag{A.4}$$

The method relies on the fact that at any time we need to compute the GW energy density power spectrum, we fourier transform u_{ij} fields and then project them using eq. (A.2). This is possible because both operations commute, therefore it is not necessary to have the source projected to TT space at every time step of evolution, which would take a very long time for the simulations as the TT projection is done in Fourier space and one would need to go back and forth between real and Fourier space.

In the lattice, the TT projection is done with an equivalent lattice projector $\Lambda^{(\mathrm{L})}_{ij,lm}$ written in terms of a lattice momentum $k_i^{(\mathrm{L})}$ which depends on the choice of spatial-derivative, see [143] for a discussion. We use the nearest-neighbor derivative of equation (71) in [135], for which the lattice momenta is given by

$$k_i^{(L)} = 2\frac{\sin(\pi\tilde{n}_i/N)}{dx}\,. \tag{A.5}$$

B Frequency and amplitude of the SGWB today

The Stochastic Gravitational Wave Background (SGWB) today is obtained by redshifting the amplitude and frequency of the background from the end of GWs production, t_{end}, following the appropriate expansion history of the Universe. We know the expansion history up to the final time t_{f} of our simulations, and noticing that $t_{\mathrm{end}} < t_{\mathrm{f}}$, we can redshift from t_{f} until the present time t_0. Let us characterize the expansion history between t_{f} and the onset of radiation domination (RD) at t_{RD}, with an effective equation of state $\bar{w} = p/\rho$

$$\log\left(\frac{\rho_{\mathrm{tot}}^{(\mathrm{RD})}}{\rho_{\mathrm{tot}}^{(\mathrm{f})}}\right) = -3\int_{a_{\mathrm{f}}}^{a_{\mathrm{RD}}}\frac{da'}{a'}(1+w(a'))\,, \tag{B.1}$$

$$= -3(1+\bar{w})\log\left(\frac{a_{\mathrm{RD}}}{a_{\mathrm{f}}}\right)\,. \tag{B.2}$$

JCAP05(2023)023

The SGWB spectrum actually peaks at some sub-horizon scale $k_p = \beta_p a_{\rm f} H_{\rm f}$, with $a_{\rm f} = a(t_{\rm f})$ and $H_{\rm f} = H(t_{\rm f})$. We expect the SGWB spectrum to peak therefore at a frequency $f_{\rm GW}$ today

$$\begin{aligned} f_{\rm GW} &\equiv \frac{k_{\rm GW}}{2\pi a_0} = \frac{\beta_{\rm GW}}{2\pi}\left(\frac{a_{\rm f}}{a_{\rm RD}}\right)\left(\frac{a_{\rm RD}}{a_0}\right) H_{\rm f} \\ &= \frac{k_{\rm GW}}{a_{\rm f} H_{\rm f}} \epsilon_{\rm f}^{1/4} G_{\rm RD}^{1/4} \left(\frac{H_{\rm f}}{m_p}\right)^{1/2} \left(\frac{2}{3}\right)^{1/4} \frac{\rho_{\rm rad,0}^{1/4}}{2\pi}\,, \end{aligned} \tag{B.3}$$

where we have defined

$$\epsilon_{\rm f} \equiv \left(\frac{a_{\rm f}}{a_{\rm RD}}\right)^{1-3\bar{w}}\,, \quad G_{\rm RD} \equiv \left(\frac{g_{\rm RD}}{g_0}\right)\left(\frac{g_{s,0}}{g_{s,RD}}\right)^{4/3}, \tag{B.4}$$

with g_s and g the entropic and energy density relativistic degrees of freedom. We can characterize the factor $G_{\rm RD}^{1/4}$ by taking into account that the SM degrees of freedom above the electroweak scale amount to $g_{s,RD} = g_{\rm RD} = 106.75$, so we write $G_{\rm RD}^{1/4} \simeq 0.7464 (g_{s,RD}/100)^{-1/12}$. The redshift factor finally reads, using $\rho_{\rm rad,0} = 3.37 \times 10^{-51} {\rm GeV}^4$,

$$f_{\rm GW} \simeq 4 \times 10^{10}\, \epsilon_{\rm f}^{\frac{1}{4}} \left(\frac{g_{\rm s,RD}}{100}\right)^{-\frac{1}{12}} \frac{k_{\rm GW}}{a_{\rm f} H_{\rm f}} \left(\frac{H_{\rm f}}{m_p}\right)^{\frac{1}{2}} {\rm Hz}\,. \tag{B.5}$$

The redshifted GW spectrum amplitude is

$$h_0^2 \Omega_{\rm GW}^{(0)}(f) = \epsilon_{\rm f}\, G_{\rm RD}\, h_0^2 \Omega_{\rm rad}^{(0)}\, \Omega_{\rm GW}(k)\,, \tag{B.6}$$

and using the value of $h_0^2 \Omega_{\rm rad}^{(0)} \approx 4 \times 10^{-5}$, the peak amplitude of the spectrum today is

$$h_0^2 \Omega_{\rm GW}^{(0)}\Big|_{\rm peak} \simeq 1.6 \times 10^{-5}\, \epsilon_{\rm f} \left(\frac{g_{\rm s,RD}}{100}\right)^{-1/3} \Omega_{\rm GW}^{(\rm p)}\,. \tag{B.7}$$

References

[1] Planck collaboration, *Planck 2018 results. X. Constraints on inflation*, *Astron. Astrophys.* **641** (2020) A10 [arXiv:1807.06211] [INSPIRE].

[2] A.H. Guth, *The Inflationary Universe: A Possible Solution to the Horizon and Flatness Problems*, *Phys. Rev. D* **23** (1981) 347 [INSPIRE].

[3] A.D. Linde, *A New Inflationary Universe Scenario: A Possible Solution of the Horizon, Flatness, Homogeneity, Isotropy and Primordial Monopole Problems*, *Phys. Lett. B* **108** (1982) 389 [INSPIRE].

[4] A.A. Starobinsky, *A New Type of Isotropic Cosmological Models Without Singularity*, *Phys. Lett. B* **91** (1980) 99 [INSPIRE].

[5] V.F. Mukhanov and G.V. Chibisov, *Quantum Fluctuations and a Nonsingular Universe*, *JETP Lett.* **33** (1981) 532 [INSPIRE].

[6] A.H. Guth and S.Y. Pi, *Fluctuations in the New Inflationary Universe*, *Phys. Rev. Lett.* **49** (1982) 1110 [INSPIRE].

[7] A.A. Starobinsky, *Dynamics of Phase Transition in the New Inflationary Universe Scenario and Generation of Perturbations*, *Phys. Lett. B* **117** (1982) 175 [INSPIRE].

JCAP05(2023)023

[8] S.W. Hawking, *The Development of Irregularities in a Single Bubble Inflationary Universe*, *Phys. Lett. B* **115** (1982) 295 [INSPIRE].

[9] J.M. Bardeen, P.J. Steinhardt and M.S. Turner, *Spontaneous Creation of Almost Scale-Free Density Perturbations in an Inflationary Universe*, *Phys. Rev. D* **28** (1983) 679 [INSPIRE].

[10] D.H. Lyth and A. Riotto, *Particle physics models of inflation and the cosmological density perturbation*, *Phys. Rept.* **314** (1999) 1 [hep-ph/9807278] [INSPIRE].

[11] A. Riotto, *Inflation and the theory of cosmological perturbations*, *ICTP Lect. Notes Ser.* **14** (2003) 317 [hep-ph/0210162] [INSPIRE].

[12] B.A. Bassett, S. Tsujikawa and D. Wands, *Inflation dynamics and reheating*, *Rev. Mod. Phys.* **78** (2006) 537 [astro-ph/0507632] [INSPIRE].

[13] A.D. Linde, *Inflationary Cosmology*, *Lect. Notes Phys.* **738** (2008) 1 [arXiv:0705.0164] [INSPIRE].

[14] D. Baumann, *Inflation*, in the proceedings of the *Theoretical Advanced Study Institute in Elementary Particle Physics: Physics of the Large and the Small*, Boulder, Colorado, U.S.A., 1–26 June 2009, p. 523–686 [DOI:10.1142/9789814327183_0010] [arXiv:0907.5424] [INSPIRE].

[15] J. Martin, C. Ringeval and V. Vennin, *Encyclopædia Inflationaris*, *Phys. Dark Univ.* **5–6** (2014) 75 [arXiv:1303.3787] [INSPIRE].

[16] BICEP and Keck collaborations, *Improved Constraints on Primordial Gravitational Waves using Planck, WMAP, and BICEP/Keck Observations through the 2018 Observing Season*, *Phys. Rev. Lett.* **127** (2021) 151301 [arXiv:2110.00483] [INSPIRE].

[17] M. Kawasaki, K. Kohri and N. Sugiyama, *Cosmological constraints on late time entropy production*, *Phys. Rev. Lett.* **82** (1999) 4168 [astro-ph/9811437] [INSPIRE].

[18] M. Kawasaki, K. Kohri and N. Sugiyama, *MeV scale reheating temperature and thermalization of neutrino background*, *Phys. Rev. D* **62** (2000) 023506 [astro-ph/0002127] [INSPIRE].

[19] S. Hannestad, *What is the lowest possible reheating temperature?*, *Phys. Rev. D* **70** (2004) 043506 [astro-ph/0403291] [INSPIRE].

[20] T. Hasegawa et al., *MeV-scale reheating temperature and thermalization of oscillating neutrinos by radiative and hadronic decays of massive particles*, *JCAP* **12** (2019) 012 [arXiv:1908.10189] [INSPIRE].

[21] J.H. Traschen and R.H. Brandenberger, *Particle Production During Out-of-equilibrium Phase Transitions*, *Phys. Rev. D* **42** (1990) 2491 [INSPIRE].

[22] L. Kofman, A.D. Linde and A.A. Starobinsky, *Reheating after inflation*, *Phys. Rev. Lett.* **73** (1994) 3195 [hep-th/9405187] [INSPIRE].

[23] Y. Shtanov, J.H. Traschen and R.H. Brandenberger, *Universe reheating after inflation*, *Phys. Rev. D* **51** (1995) 5438 [hep-ph/9407247] [INSPIRE].

[24] D.I. Kaiser, *Post inflation reheating in an expanding universe*, *Phys. Rev. D* **53** (1996) 1776 [astro-ph/9507108] [INSPIRE].

[25] L. Kofman, A.D. Linde and A.A. Starobinsky, *Towards the theory of reheating after inflation*, *Phys. Rev. D* **56** (1997) 3258 [hep-ph/9704452] [INSPIRE].

[26] P.B. Greene, L. Kofman, A.D. Linde and A.A. Starobinsky, *Structure of resonance in preheating after inflation*, *Phys. Rev. D* **56** (1997) 6175 [hep-ph/9705347] [INSPIRE].

[27] D.I. Kaiser, *Preheating in an expanding universe: Analytic results for the massless case*, *Phys. Rev. D* **56** (1997) 706 [hep-ph/9702244] [INSPIRE].

[28] D.I. Kaiser, *Resonance structure for preheating with massless fields*, *Phys. Rev. D* **57** (1998) 702 [hep-ph/9707516] [INSPIRE].

JCAP05(2023)023

[29] J.F. Dufaux et al., *Preheating with trilinear interactions: Tachyonic resonance*, *JCAP* **07** (2006) 006 [hep-ph/0602144] [INSPIRE].

[30] D. Croon, V. Sanz and E.R.M. Tarrant, *Reheating with a composite Higgs boson*, *Phys. Rev. D* **94** (2016) 045010 [arXiv:1507.04653] [INSPIRE].

[31] S. Antusch, F. Cefala, D. Nolde and S. Orani, *Parametric resonance after hilltop inflation caused by an inhomogeneous inflaton field*, *JCAP* **02** (2016) 044 [arXiv:1510.04856] [INSPIRE].

[32] K. Enqvist et al., *Postinflationary vacuum instability and Higgs-inflaton couplings*, *JCAP* **11** (2016) 025 [arXiv:1608.08848] [INSPIRE].

[33] B.A. Bassett and S. Liberati, *Geometric reheating after inflation*, *Phys. Rev. D* **58** (1998) 021302 [*Erratum ibid.* **60** (1999) 049902] [hep-ph/9709417] [INSPIRE].

[34] S. Tsujikawa, K.-I. Maeda and T. Torii, *Resonant particle production with nonminimally coupled scalar fields in preheating after inflation*, *Phys. Rev. D* **60** (1999) 063515 [hep-ph/9901306] [INSPIRE].

[35] C. Fu, P. Wu and H. Yu, *Nonlinear preheating with nonminimally coupled scalar fields in the Starobinsky model*, *Phys. Rev. D* **99** (2019) 123526 [arXiv:1906.00557] [INSPIRE].

[36] D.G. Figueroa, A. Florio, T. Opferkuch and B.A. Stefanek, *Dynamics of Non-minimally Coupled Scalar Fields in the Jordan Frame*, arXiv:2112.08388 [INSPIRE].

[37] G.N. Felder et al., *Dynamics of symmetry breaking and tachyonic preheating*, *Phys. Rev. Lett.* **87** (2001) 011601 [hep-ph/0012142] [INSPIRE].

[38] G.N. Felder, L. Kofman and A.D. Linde, *Tachyonic instability and dynamics of spontaneous symmetry breaking*, *Phys. Rev. D* **64** (2001) 123517 [hep-th/0106179] [INSPIRE].

[39] J. Garcia-Bellido, M. Garcia Perez and A. Gonzalez-Arroyo, *Symmetry breaking and false vacuum decay after hybrid inflation*, *Phys. Rev. D* **67** (2003) 103501 [hep-ph/0208228] [INSPIRE].

[40] E.J. Copeland, S. Pascoli and A. Rajantie, *Dynamics of tachyonic preheating after hybrid inflation*, *Phys. Rev. D* **65** (2002) 103517 [hep-ph/0202031] [INSPIRE].

[41] A. Rajantie, P.M. Saffin and E.J. Copeland, *Electroweak preheating on a lattice*, *Phys. Rev. D* **63** (2001) 123512 [hep-ph/0012097] [INSPIRE].

[42] E.J. Copeland, D. Lyth, A. Rajantie and M. Trodden, *Hybrid inflation and baryogenesis at the TeV scale*, *Phys. Rev. D* **64** (2001) 043506 [hep-ph/0103231] [INSPIRE].

[43] J. Smit and A. Tranberg, *Chern-Simons number asymmetry from CP violation at electroweak tachyonic preheating*, *JHEP* **12** (2002) 020 [hep-ph/0211243] [INSPIRE].

[44] J. Garcia-Bellido, M. Garcia-Perez and A. Gonzalez-Arroyo, *Chern-Simons production during preheating in hybrid inflation models*, *Phys. Rev. D* **69** (2004) 023504 [hep-ph/0304285] [INSPIRE].

[45] A. Tranberg and J. Smit, *Baryon asymmetry from electroweak tachyonic preheating*, *JHEP* **11** (2003) 016 [hep-ph/0310342] [INSPIRE].

[46] J.-I. Skullerud, J. Smit and A. Tranberg, *W and Higgs particle distributions during electroweak tachyonic preheating*, *JHEP* **08** (2003) 045 [hep-ph/0307094] [INSPIRE].

[47] M. van der Meulen, D. Sexty, J. Smit and A. Tranberg, *Chern-Simons and winding number in a tachyonic electroweak transition*, *JHEP* **02** (2006) 029 [hep-ph/0511080] [INSPIRE].

[48] A. Diaz-Gil, J. Garcia-Bellido, M. Garcia Perez and A. Gonzalez-Arroyo, *Magnetic field production during preheating at the electroweak scale*, *Phys. Rev. Lett.* **100** (2008) 241301 [arXiv:0712.4263] [INSPIRE].

JCAP05(2023)023

[49] A. Diaz-Gil, J. Garcia-Bellido, M. Garcia Perez and A. Gonzalez-Arroyo, *Primordial magnetic fields from preheating at the electroweak scale*, *JHEP* **07** (2008) 043 [arXiv:0805.4159] [INSPIRE].

[50] J.-F. Dufaux, D.G. Figueroa and J. Garcia-Bellido, *Gravitational Waves from Abelian Gauge Fields and Cosmic Strings at Preheating*, *Phys. Rev. D* **82** (2010) 083518 [arXiv:1006.0217] [INSPIRE].

[51] A. Tranberg, S. Tähtinen and D.J. Weir, *Gravitational waves from non-Abelian gauge fields at a tachyonic transition*, *JCAP* **04** (2018) 012 [arXiv:1706.02365] [INSPIRE].

[52] P. Adshead, J.T. Giblin, T.R. Scully and E.I. Sfakianakis, *Gauge-preheating and the end of axion inflation*, *JCAP* **12** (2015) 034 [arXiv:1502.06506] [INSPIRE].

[53] J.R.C. Cuissa and D.G. Figueroa, *Lattice formulation of axion inflation. Application to preheating*, *JCAP* **06** (2019) 002 [arXiv:1812.03132] [INSPIRE].

[54] P. Adshead, J.T. Giblin, M. Pieroni and Z.J. Weiner, *Constraining axion inflation with gravitational waves from preheating*, *Phys. Rev. D* **101** (2020) 083534 [arXiv:1909.12842] [INSPIRE].

[55] Y. Cui and E.I. Sfakianakis, *Detectable gravitational wave signals from inflationary preheating*, *Phys. Lett. B* **840** (2023) 137825 [arXiv:2112.00762] [INSPIRE].

[56] F. Bezrukov, D. Gorbunov and M. Shaposhnikov, *On initial conditions for the Hot Big Bang*, *JCAP* **06** (2009) 029 [arXiv:0812.3622] [INSPIRE].

[57] J. Garcia-Bellido, D.G. Figueroa and J. Rubio, *Preheating in the Standard Model with the Higgs-Inflaton coupled to gravity*, *Phys. Rev. D* **79** (2009) 063531 [arXiv:0812.4624] [INSPIRE].

[58] J. Braden, L. Kofman and N. Barnaby, *Reheating the Universe After Multi-Field Inflation*, *JCAP* **07** (2010) 016 [arXiv:1005.2196] [INSPIRE].

[59] J.T. Giblin Jr., L.R. Price and X. Siemens, *Gravitational Radiation from Preheating with Many Fields*, *JCAP* **08** (2010) 012 [arXiv:1006.0935] [INSPIRE].

[60] D.G. Figueroa, A. Florio, N. Loayza and M. Pieroni, *Spectroscopy of particle couplings with gravitational waves*, *Phys. Rev. D* **106** (2022) 063522 [arXiv:2202.05805] [INSPIRE].

[61] M.P. DeCross et al., *Preheating after Multifield Inflation with Nonminimal Couplings, I: Covariant Formalism and Attractor Behavior*, *Phys. Rev. D* **97** (2018) 023526 [arXiv:1510.08553] [INSPIRE].

[62] M.P. DeCross et al., *Preheating after multifield inflation with nonminimal couplings, II: Resonance Structure*, *Phys. Rev. D* **97** (2018) 023527 [arXiv:1610.08868] [INSPIRE].

[63] M.P. DeCross et al., *Preheating after multifield inflation with nonminimal couplings, III: Dynamical spacetime results*, *Phys. Rev. D* **97** (2018) 023528 [arXiv:1610.08916] [INSPIRE].

[64] T. Krajewski, K. Turzyński and M. Wieczorek, *On preheating in α-attractor models of inflation*, *Eur. Phys. J. C* **79** (2019) 654 [arXiv:1801.01786] [INSPIRE].

[65] O. Iarygina, E.I. Sfakianakis, D.-G. Wang and A. Achucarro, *Universality and scaling in multi-field α-attractor preheating*, *JCAP* **06** (2019) 027 [arXiv:1810.02804] [INSPIRE].

[66] R. Allahverdi, R. Brandenberger, F.-Y. Cyr-Racine and A. Mazumdar, *Reheating in Inflationary Cosmology: Theory and Applications*, *Ann. Rev. Nucl. Part. Sci.* **60** (2010) 27 [arXiv:1001.2600] [INSPIRE].

[67] M.A. Amin, M.P. Hertzberg, D.I. Kaiser and J. Karouby, *Nonperturbative Dynamics Of Reheating After Inflation: A Review*, *Int. J. Mod. Phys. D* **24** (2014) 1530003 [arXiv:1410.3808] [INSPIRE].

[68] K.D. Lozanov, *Lectures on Reheating after Inflation*, arXiv:1907.04402 [INSPIRE].

JCAP05(2023)023

[69] R. Allahverdi et al., *The First Three Seconds: a Review of Possible Expansion Histories of the Early Universe*, arXiv:2006.16182 [DOI:10.21105/astro.2006.16182] [INSPIRE].

[70] L.P. Grishchuk, *Amplification of gravitational waves in an istropic universe*, *Zh. Eksp. Teor. Fiz.* **67** (1974) 825 [INSPIRE].

[71] A.A. Starobinsky, *Spectrum of relict gravitational radiation and the early state of the universe*, *JETP Lett.* **30** (1979) 682 [INSPIRE].

[72] V.A. Rubakov, M.V. Sazhin and A.V. Veryaskin, *Graviton Creation in the Inflationary Universe and the Grand Unification Scale*, *Phys. Lett. B* **115** (1982) 189 [INSPIRE].

[73] R. Fabbri and M. Pollock, *The Effect of Primordially Produced Gravitons upon the Anisotropy of the Cosmological Microwave Background Radiation*, *Phys. Lett. B* **125** (1983) 445 [INSPIRE].

[74] K. Saikawa and S. Shirai, *Primordial gravitational waves, precisely: The role of thermodynamics in the Standard Model*, *JCAP* **05** (2018) 035 [arXiv:1803.01038] [INSPIRE].

[75] T. Kite, J. Chluba, A. Ravenni and S.P. Patil, *Clarifying transfer function approximations for the large-scale gravitational wave background in ΛCDM*, *Mon. Not. Roy. Astron. Soc.* **509** (2021) 1366 [arXiv:2107.13351] [INSPIRE].

[76] M.M. Anber and L. Sorbo, *N-flationary magnetic fields*, *JCAP* **10** (2006) 018 [astro-ph/0606534] [INSPIRE].

[77] L. Sorbo, *Parity violation in the Cosmic Microwave Background from a pseudoscalar inflaton*, *JCAP* **06** (2011) 003 [arXiv:1101.1525] [INSPIRE].

[78] E. Pajer and M. Peloso, *A review of Axion Inflation in the era of Planck*, *Class. Quant. Grav.* **30** (2013) 214002 [arXiv:1305.3557] [INSPIRE].

[79] P. Adshead, E. Martinec and M. Wyman, *Gauge fields and inflation: Chiral gravitational waves, fluctuations, and the Lyth bound*, *Phys. Rev. D* **88** (2013) 021302 [arXiv:1301.2598] [INSPIRE].

[80] P. Adshead, E. Martinec and M. Wyman, *Perturbations in Chromo-Natural Inflation*, *JHEP* **09** (2013) 087 [arXiv:1305.2930] [INSPIRE].

[81] A. Maleknejad, *Axion Inflation with an* SU(2) *Gauge Field: Detectable Chiral Gravity Waves*, *JHEP* **07** (2016) 104 [arXiv:1604.03327] [INSPIRE].

[82] E. Dimastrogiovanni, M. Fasiello and T. Fujita, *Primordial Gravitational Waves from Axion-Gauge Fields Dynamics*, *JCAP* **01** (2017) 019 [arXiv:1608.04216] [INSPIRE].

[83] R. Namba et al., *Scale-dependent gravitational waves from a rolling axion*, *JCAP* **01** (2016) 041 [arXiv:1509.07521] [INSPIRE].

[84] R.Z. Ferreira, J. Ganc, J. Noreña and M.S. Sloth, *On the validity of the perturbative description of axions during inflation*, *JCAP* **04** (2016) 039 [*Erratum ibid.* **10** (2016) E01] [arXiv:1512.06116] [INSPIRE].

[85] M. Peloso, L. Sorbo and C. Unal, *Rolling axions during inflation: perturbativity and signatures*, *JCAP* **09** (2016) 001 [arXiv:1606.00459] [INSPIRE].

[86] V. Domcke, M. Pieroni and P. Binétruy, *Primordial gravitational waves for universality classes of pseudoscalar inflation*, *JCAP* **06** (2016) 031 [arXiv:1603.01287] [INSPIRE].

[87] R.R. Caldwell and C. Devulder, *Axion Gauge Field Inflation and Gravitational Leptogenesis: A Lower Bound on B Modes from the Matter-Antimatter Asymmetry of the Universe*, *Phys. Rev. D* **97** (2018) 023532 [arXiv:1706.03765] [INSPIRE].

[88] M.C. Guzzetti, N. Bartolo, M. Liguori and S. Matarrese, *Gravitational waves from inflation*, *Riv. Nuovo Cim.* **39** (2016) 399 [arXiv:1605.01615] [INSPIRE].

[89] N. Bartolo et al., *Science with the space-based interferometer LISA. IV: Probing inflation with gravitational waves*, *JCAP* **12** (2016) 026 [arXiv:1610.06481] [INSPIRE].

JCAP05(2023)023

[90] R. Easther and E.A. Lim, *Stochastic gravitational wave production after inflation*, *JCAP* **04** (2006) 010 [astro-ph/0601617] [INSPIRE].

[91] J. Garcia-Bellido and D.G. Figueroa, *A stochastic background of gravitational waves from hybrid preheating*, *Phys. Rev. Lett.* **98** (2007) 061302 [astro-ph/0701014] [INSPIRE].

[92] J. Garcia-Bellido, D.G. Figueroa and A. Sastre, *A Gravitational Wave Background from Reheating after Hybrid Inflation*, *Phys. Rev. D* **77** (2008) 043517 [arXiv:0707.0839] [INSPIRE].

[93] J.F. Dufaux et al., *Theory and Numerics of Gravitational Waves from Preheating after Inflation*, *Phys. Rev. D* **76** (2007) 123517 [arXiv:0707.0875] [INSPIRE].

[94] J.-F. Dufaux, G. Felder, L. Kofman and O. Navros, *Gravity Waves from Tachyonic Preheating after Hybrid Inflation*, *JCAP* **03** (2009) 001 [arXiv:0812.2917] [INSPIRE].

[95] L. Bethke, D.G. Figueroa and A. Rajantie, *Anisotropies in the Gravitational Wave Background from Preheating*, *Phys. Rev. Lett.* **111** (2013) 011301 [arXiv:1304.2657] [INSPIRE].

[96] L. Bethke, D.G. Figueroa and A. Rajantie, *On the Anisotropy of the Gravitational Wave Background from Massless Preheating*, *JCAP* **06** (2014) 047 [arXiv:1309.1148] [INSPIRE].

[97] D.G. Figueroa and F. Torrenti, *Gravitational wave production from preheating: parameter dependence*, *JCAP* **10** (2017) 057 [arXiv:1707.04533] [INSPIRE].

[98] P. Adshead, J.T. Giblin and Z.J. Weiner, *Gravitational waves from gauge preheating*, *Phys. Rev. D* **98** (2018) 043525 [arXiv:1805.04550] [INSPIRE].

[99] P. Adshead, J.T. Giblin, M. Pieroni and Z.J. Weiner, *Constraining Axion Inflation with Gravitational Waves across 29 Decades in Frequency*, *Phys. Rev. Lett.* **124** (2020) 171301 [arXiv:1909.12843] [INSPIRE].

[100] S.-Y. Zhou et al., *Gravitational Waves from Oscillon Preheating*, *JHEP* **10** (2013) 026 [arXiv:1304.6094] [INSPIRE].

[101] S. Antusch, F. Cefala and S. Orani, *Gravitational waves from oscillons after inflation*, *Phys. Rev. Lett.* **118** (2017) 011303 [*Erratum ibid.* **120** (2018) 219901] [arXiv:1607.01314] [INSPIRE].

[102] S. Antusch, F. Cefala and S. Orani, *What can we learn from the stochastic gravitational wave background produced by oscillons?*, *JCAP* **03** (2018) 032 [arXiv:1712.03231] [INSPIRE].

[103] J. Liu, Z.-K. Guo, R.-G. Cai and G. Shiu, *Gravitational Waves from Oscillons with Cuspy Potentials*, *Phys. Rev. Lett.* **120** (2018) 031301 [arXiv:1707.09841] [INSPIRE].

[104] M.A. Amin et al., *Gravitational waves from asymmetric oscillon dynamics?*, *Phys. Rev. D* **98** (2018) 024040 [arXiv:1803.08047] [INSPIRE].

[105] M. Giovannini, *Gravitational waves constraints on postinflationary phases stiffer than radiation*, *Phys. Rev. D* **58** (1998) 083504 [hep-ph/9806329] [INSPIRE].

[106] M. Giovannini, *Production and detection of relic gravitons in quintessential inflationary models*, *Phys. Rev. D* **60** (1999) 123511 [astro-ph/9903004] [INSPIRE].

[107] L.A. Boyle and A. Buonanno, *Relating gravitational wave constraints from primordial nucleosynthesis, pulsar timing, laser interferometers, and the CMB: Implications for the early Universe*, *Phys. Rev. D* **78** (2008) 043531 [arXiv:0708.2279] [INSPIRE].

[108] D.G. Figueroa and E.H. Tanin, *Inconsistency of an inflationary sector coupled only to Einstein gravity*, *JCAP* **10** (2019) 050 [arXiv:1811.04093] [INSPIRE].

[109] D.G. Figueroa and E.H. Tanin, *Ability of LIGO and LISA to probe the equation of state of the early Universe*, *JCAP* **08** (2019) 011 [arXiv:1905.11960] [INSPIRE].

[110] Y. Gouttenoire, G. Servant and P. Simakachorn, *Kination cosmology from scalar fields and gravitational-wave signatures*, arXiv:2111.01150 [INSPIRE].

JCAP05(2023)023

[111] R.T. Co et al., *Gravitational wave and CMB probes of axion kination*, *JHEP* **09** (2022) 116 [arXiv:2108.09299] [INSPIRE].

[112] C. Caprini and D.G. Figueroa, *Cosmological Backgrounds of Gravitational Waves*, *Class. Quant. Grav.* **35** (2018) 163001 [arXiv:1801.04268] [INSPIRE].

[113] M. Maggiore, *Gravitational Waves. Vol. 2: Astrophysics and Cosmology*, Oxford University Press (2018) [INSPIRE].

[114] D.G. Figueroa and F. Torrenti, *Parametric resonance in the early Universe — a fitting analysis*, *JCAP* **02** (2017) 001 [arXiv:1609.05197] [INSPIRE].

[115] S. Antusch, D.G. Figueroa, K. Marschall and F. Torrenti, *Energy distribution and equation of state of the early Universe: matching the end of inflation and the onset of radiation domination*, *Phys. Lett. B* **811** (2020) 135888 [arXiv:2005.07563] [INSPIRE].

[116] S. Antusch, D.G. Figueroa, K. Marschall and F. Torrenti, *Characterizing the postinflationary reheating history: Single daughter field with quadratic-quadratic interaction*, *Phys. Rev. D* **105** (2022) 043532 [arXiv:2112.11280] [INSPIRE].

[117] S. Antusch, K. Marschall and F. Torrenti, *Characterizing the post-inflationary reheating history. Part II. Multiple interacting daughter fields*, *JCAP* **02** (2023) 019 [arXiv:2206.06319] [INSPIRE].

[118] A.D. Dolgov and A.D. Linde, *Baryon Asymmetry in Inflationary Universe*, *Phys. Lett. B* **116** (1982) 329 [INSPIRE].

[119] L.F. Abbott, E. Farhi and M.B. Wise, *Particle Production in the New Inflationary Cosmology*, *Phys. Lett. B* **117** (1982) 29 [INSPIRE].

[120] P.B. Greene and L. Kofman, *Preheating of fermions*, *Phys. Lett. B* **448** (1999) 6 [hep-ph/9807339] [INSPIRE].

[121] P.B. Greene and L. Kofman, *On the theory of fermionic preheating*, *Phys. Rev. D* **62** (2000) 123516 [hep-ph/0003018] [INSPIRE].

[122] M. Peloso and L. Sorbo, *Preheating of massive fermions after inflation: Analytical results*, *JHEP* **05** (2000) 016 [hep-ph/0003045] [INSPIRE].

[123] J. Berges, D. Gelfand and J. Pruschke, *Quantum theory of fermion production after inflation*, *Phys. Rev. Lett.* **107** (2011) 061301 [arXiv:1012.4632] [INSPIRE].

[124] Y. Ema et al., *Higgs-inflaton mixing and vacuum stability*, *Phys. Lett. B* **789** (2019) 373 [arXiv:1711.10554] [INSPIRE].

[125] G. Degrassi et al., *Higgs mass and vacuum stability in the Standard Model at NNLO*, *JHEP* **08** (2012) 098 [arXiv:1205.6497] [INSPIRE].

[126] F. Bezrukov, M.Y. Kalmykov, B.A. Kniehl and M. Shaposhnikov, *Higgs Boson Mass and New Physics*, *JHEP* **10** (2012) 140 [arXiv:1205.2893] [INSPIRE].

[127] Planck collaboration, *Planck 2018 results. VI. Cosmological parameters*, *Astron. Astrophys.* **641** (2020) A6 [*Erratum ibid.* **652** (2021) C4] [arXiv:1807.06209] [INSPIRE].

[128] L. Pagano, L. Salvati and A. Melchiorri, *New constraints on primordial gravitational waves from Planck 2015*, *Phys. Lett. B* **760** (2016) 823 [arXiv:1508.02393] [INSPIRE].

[129] K. Abazajian et al., *CMB-S4 Science Case, Reference Design, and Project Plan*, arXiv:1907.04473 [INSPIRE].

[130] COrE collaboration, *COrE (Cosmic Origins Explorer) A White Paper*, arXiv:1102.2181 [INSPIRE].

[131] EUCLID collaboration, *Euclid Definition Study Report*, arXiv:1110.3193 [INSPIRE].

JCAP05(2023)023

[132] S. Tsujikawa, J. Ohashi, S. Kuroyanagi and A. De Felice, *Planck constraints on single-field inflation*, *Phys. Rev. D* **88** (2013) 023529 [arXiv:1305.3044] [INSPIRE].

[133] R. Kallosh and A. Linde, *Universality Class in Conformal Inflation*, *JCAP* **07** (2013) 002 [arXiv:1306.5220] [INSPIRE].

[134] M.S. Turner, *Coherent Scalar Field Oscillations in an Expanding Universe*, *Phys. Rev. D* **28** (1983) 1243 [INSPIRE].

[135] D.G. Figueroa, A. Florio, F. Torrenti and W. Valkenburg, *The art of simulating the early Universe — Part I*, *JCAP* **04** (2021) 035 [arXiv:2006.15122] [INSPIRE].

[136] D.G. Figueroa, A. Florio, F. Torrenti and W. Valkenburg, *CosmoLattice: A modern code for lattice simulations of scalar and gauge field dynamics in an expanding universe*, *Comput. Phys. Commun.* **283** (2023) 108586 [arXiv:2102.01031] [INSPIRE].

[137] *Cosmolattice: Gravitational Waves*, https://cosmolattice.net/assets/technical_notes/CosmoLattice_TechnicalNote_GWs.pdf.

[138] N. Aggarwal et al., *Challenges and opportunities of gravitational-wave searches at MHz to GHz frequencies*, *Living Rev. Rel.* **24** (2021) 4 [arXiv:2011.12414] [INSPIRE].

[139] J.J. Bennett et al., *Towards a precision calculation of $N_{\rm eff}$ in the Standard Model II: Neutrino decoupling in the presence of flavour oscillations and finite-temperature QED*, *JCAP* **04** (2021) 073 [arXiv:2012.02726] [INSPIRE].

[140] I. Ben-Dayan, B. Keating, D. Leon and I. Wolfson, *Constraints on scalar and tensor spectra from $N_{\rm eff}$*, *JCAP* **06** (2019) 007 [arXiv:1903.11843] [INSPIRE].

[141] M. Drees and Y. Xu, *Small field polynomial inflation: reheating, radiative stability and lower bound*, *JCAP* **09** (2021) 012 [arXiv:2104.03977] [INSPIRE].

[142] N. Bernal and Y. Xu, *Polynomial inflation and dark matter*, *Eur. Phys. J. C* **81** (2021) 877 [arXiv:2106.03950] [INSPIRE].

[143] D.G. Figueroa, J. Garcia-Bellido and A. Rajantie, *On the Transverse-Traceless Projection in Lattice Simulations of Gravitational Wave Production*, *JCAP* **11** (2011) 015 [arXiv:1110.0337] [INSPIRE].

JCAP05(2023)023